The Digital Design and Synthesis of Delay Doppler Maps

in GNSS Remote Sensing Receivers

Giovanna Franco

A Thesis

in

The Department

of

Electrical and Computer Engineering

Presented in Partial Fulfillment of the Requirements

for the Degree of Master of Applied Science (Electrical and Computer Engineering) at

Concordia University

Montreal, Quebec, Canada

August 2013

CONCORDIA UNIVERSITY
SCHOOL OF GRADUATE STUDIES

This is to certify that the thesis prepared

By: Giovanna Franco

Entitled: "The Digital Design and Synthesis of Delay Doppler Maps in GNSS
          Remote Sensing Receivers"

and submitted in partial fulfillment of the requirements for the degree of

Master of Applied Science

Complies with the regulations of this University and meets the accepted standards with
respect to originality and quality.

Signed by the final examining committee:

_____ Chair
        Dr. M. Z. Kabir

_____ Examiner, External
        Dr. A. Ben Hamza (CIISE)   To the Program

_____ Examiner
        Dr. R. Paknys

_____ Supervisor
        Dr. S. Gleason

Approved by: _____
            Dr. W. E. Lynch, Chair
      Department of Electrical and Computer Engineering

_____20_____   _____
                              Dr. C. W. Trueman
                        Interim Dean, Faculty of Engineering
                          and Computer Science

ABSTRACT

The Digital Design and Synthesis of Delay Doppler Maps

in GNSS Remote Sensing Receivers

Giovanna Franco, M.A.Sc Candidate

Global Navigation Satellite Systems (GNSS) are satellite based systems primarily capable of determining the location of receivers on the Earth. However, these systems can also receive and process bistatically surface reflected signals, studying the scattering from the signal off the reflection surface. In order to achieve these results, accurate and fast technology are necessary. In this work, a Delay-Doppler mapping module of a GNSS system has been implemented in VHDL and synthesized on FPGA Xilinx-Virtex 6 to map the delay and frequency domains of Earth scattered signals. The designed system presents high timing performance to provide quick and accurate measurements. In this work, a FFT based GNSS mapping algorithms has been designed to process raw samples GNSS data. The remote sensing module has been implemented, generating all the 32 possible C/A codes and then processing the received signal for each of the 32 C/A codes in a pipelined circuit. Once the GNSS power signals have been detected, a final detector is used to compare all the GNSS power signals found with a magnitude twice the noise and with the highest peak to detect the best candidate signal for the Delay Doppler Map (DDM). Different timing delay ranges and Doppler frequency ranges have been considered to compare the performance of the mapping algorithm. The use of an FPGA based algorithm permits significantly higher performance and greater flexibility than software based solutions and opens up the GNSS remote sensing application for integration into real-time instruments.

Contents

List of Figures

Chapter 1

Introduction and Background

The Global Navigation Satellite System (GNSS) is a satellite based system able to provide precise and accurate measurements of the Earth's surface environments, studying the scattering of the GNSS signal on the reflection's surface (Gleason et al. [21]). Martin-Neira presented a first theory to study the Earth reflected GNSS signals on the ocean surface in 1988 (Martin-Neira [34]) at the European Space Agency. Many contributions have been introduced to those theories by several researchers. An advanced model based on the Kirchoff approximation and geometric optics limit to study the ocean scattered GPS signals was presented by Zavorotny and Voronovich [58] in 2000, often used with the Elfouhaily's ocean wave spectrum (Elfouhaily et al. [10]).

Armatys [1] observed the changes of the GPS reflected power on ocean surface with changes in wind speed and direction. These studies were based on experiments performed on a aircraft and spacerborne platform simulations. Using the electromagnetic model of V. Zavorotny and A. Voronovich [58] and considering changing wind conditions, Armatys showed the accuracy to determine wind vector over the glistening zone. Garrison et al. [16] performed aircraft experiments to measure the reflected cross-correlation power on sea surface to estimate the wind speed. The obtained distribution power has been compared with a analytic model to test the accuracy of this method and the precision of the satellite instru-

ments. These experiments conducted in two campaigns were based on a specialized GPS receiver and on the use of correlation measurements in an inverse bi-static scattering model to retrieve wind speed information. In addition, Lowe et al. [33], Ruffini [42] brought innovative idea to measure altimetry on the reflecting surface. Due to the vast use of the Global Positioning System (GPS) technology in the GNSS, most of the subjects presented in this manuscript are labeled for GPS but they are applied to GNSS.

1.1   GNSS Remote Sensing

1.1.1   Reflection Geometry

The GNSS signals are constantly transmitted on the Earch, each of them is scattered in different direction once it meets the Earth surface. The interaction with the Earth and the reflected components of other signals produce a directional reflection of the GNSS signal. The information carried form the GNSS signal together with the information of the delay of the GNSS reflected signal, the receiver antenna position and the delay measurements associated with the scattering surface can be used to retrieve information about the reflecting surface (Gleason et al. [21]).
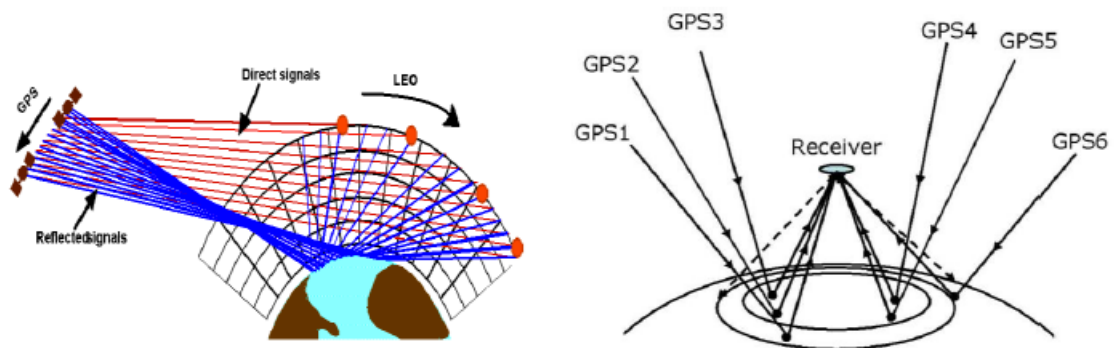
Figure 1.1: GNSS Reflection Geometry (Yunck [57])

1.1.2 GNSS Remote Sensing Applications

Ocean

The ability of the GNSS bi-static techniques to measure the ocean height, the wind speed and the scattering surface roughness and condition helps to monitor the environment's changes and prevent undesirable effects. Considering that the roughness of the ocean surface depends on the size and the shape of the glistening zone, the key issue is to measure the received power of the GNSS reflected signal (Garrison et al. [13]) (Clifford et al. [8]). In order to perform those measurements, once multiplied the received signal by a pseudo-random delayed noise sequences, the resulting waveform is detected and processed. The resulting signal is mapped respect to time delays and Doppler frequencies, able to give information about the glistening zone roughness and the wind speed.

Studies presented by Chao in 1996 [6] and Smith in 2000 [45] showed the possibility to monitor the dynamics of the ocean observing the eddies in time and space, still not supported by the traditional radar for remote sensing. For what concern the ocean altimetry, the observation of the barotropic parameters changes in space and time across represents another challenge of the GNSS system.

The GNSS-RS applied to ocean altimetry presents several advantages compared to the traditional radar. One of them is the ability to retrieve multiple reflection signals at the same time. On the other hand a more sophisticated and high-gain antennae is necessary to capture all the reflections. The receiver has the additional task of coordinating the antennae (Gleason et al. [21]).

Another application of the GNSS in remote sensing is the measurement of the wind speed from an aircraft. Armatys [1] and later Komjathy et al. [27] presented some experiments about the retrieval of the wind speed using the one-dimensional reflected GNSS signal transmitted from three GPS satellites. Other experiments have been conducted in the last years, in 2004 Soulat conducted the measurement of the ocean directional mean square

slope with two-dimensional GPS reflected signal from a single GNSS satellite at 1 km of altitude (Soulat [46]). Instead Cardellach et al. [5] developed a new algorithm to compute the PDF (*Probability Density Function*) of the ocean slopes.

In 2013, Ruf et al. [40] performed the spaceborne mission the NASA EV-2 Cyclone Global Navigation Satellite System (CYGNSS) mission to improve the accuracy of tropical cycle track forecasts. In these experiments, it is presented a method to retrieve near-surface wind speed estimation from the Delay-Doppler Map.

Land

The GPS reflected signals remote sensing could represent a valid alternative to the satellite radar, incapable to monitor small Earth's regions. The University of Colorado and NASA Langley Research Center were the pilots of the GNSS land sensing's research (Katzberg et al. [25]). The experiments involved the measurements of land surfaces retrieved from Earth fixed stations using a flying aircraft (Gleason et al. [21]). The GNSS systems are able to measure the surface height, to discriminate the soil moisture with high accuracy. The ability to acquire information about the soil conditions makes the GNSS method applicable to coastal and wetland remote sensing tool (Garrison et al. [15]).

In 2004, Dallas Masters [36] was able to observe changes on the cover of the glisting zone with GNSS remote sensing method. The GNSS techniques could allow flood prediction, draining and run-off estimations for urban planning, even though it could be changeling due to extension of the scattering area and the not homogeneous soil moisture and surface (Gleason et al. [21]). Other experiments were performed by (Gleason et al. [18]) to reduce the distortions introduced by the speckle noise on the reflected signals scattered from land surface, as well as from ocean and from ice scattering area, respectively.

Sea Ice

The GNSS system can be used to monitor sea ice surface as proved by Komjathy et al. [26] monitoring the sea ice, fresh water and frozen land condition of the Arctic sea ice performing experiments from an aircraft on the Alaska region. Other studies where conducted by Belmonte Rivas et al. [2], who analyzed the behavior of the GPS signals on scattering sea ice surface. The reflected GPS signal is sensitive to the condition of the sea, resulting in an increasing scattering zone's roughness in new formed ice. The study of the GPS reflection represents a low-cost and robust way to monitor the sea ice conditions (Belmonte Rivas et al. [2]).

In 2010, Gleason [22] conducted experiments on two different ice concentration validating the GNSS measurements with the AMSR-E (*Advanced Microwave Scanning Radiometer for Earth Observing System*) instrument ice estimation. The GNSS remote sensing on sea ice surface can be used to measure the ice thickness and coverage to monitor the icebergs and ice shelves of Greenland. This could be helpful to study the changing climate or to prevent issues in the naval transportation next to the Arctic areas (Gleason et al. [21]).

1.1.3   Research Contributions

The GNSS systems represents an efficient response to the necessity of accurate and low cost solutions for ocean altimetry, soil moisture, sea ice and snow measurements. The next generation of multi frequency GNSS satellite constellations presents a challenge for the GNSS receiver. The new GNSS systems as GPS IIF, GPS III, GLONASS, GALILEO, COMPASS establish the beginning of high-performing receivers able to measure GPS refractometry and reflectometry directly on-board. These new receivers can be aircraft, ground stations on the Earth or GPS receivers on LEO (*Low Earth Orbit*) satellites.

Considering the potential and the wide range of applications of the GNSS systems, this work has been focused on the hardware design in VHDL of the Acquisition Unit of a

GNSS system to plot the Delay Doppler Map (*DDM*) with high timing performances. The Delay-Doppler Map is an efficient tool to study the reflection of the GNSS signal on the scattering surface for a range of time delays and Doppler frequencies. Therefore, a fast Acquisition Unit is able to provide prompt information of the scattered power improving the monitoring of environment changes (Gleason et al. [21]), (Schmidt et al. [44]). The upcoming space-borne GPS reflectometry and refractometry missions will provide more accurate and detailed measurements of the ground surface characteristics, ocean altimetry and ionospheric and tropospheric processes (Gleason et al. [21]). The introduction of hardware based processed represents an significant reductions of the cost and of the processing time. An optimized design on FPGA provides an reduced occupation area, a low power consumption and the ability to reconfigure and reprogram the hardware as many times as necessary.

In a scenario where the GNSS systems are achieving detailed measurements on every kind of surface with global and local scale, it is necessary to provide devices and design which help the receiver to achieve the required results. The hardware design of digital signal processing responds to the necessity of accurate results in a sort time using small and low-cost instruments. A design on FPGA can be easily combined with DSP (*Digital Signal Processor*) (Girau et al. [17]) and programmable ASIP (*Application Specific Instruction Processor*) (Kappen et al. [24]).

In this work, the Acquisition Unit of the GNSS receiver has been implemented in VHDL and synthesized on FPGA Xilinx-Virtex6 with low timing delay and with the possibility to integrate this design in a bigger GNSS system project. The Delay-Doppler Map proves the ability of the FPGA in providing accurate measurements of the reflected power signal on the scattering surface.

1.2 Global Navigation System

The necessity to know the exact location in time and space has induced the humanity to look for new technique. Starting from the Ancient Egyptian pyramids, the civilization has developed methods to measure time and position of terrestrial targets based on the celestial observation. The Dutch Snell van Royen and the French Picard and Cassini were one of the first to study *the triangulation* technique to compute accurate coordinates on the Earth. Due to its lack of accuracy, the triangulation was soon replaced by *the trilateration*. Used for the first times in the World War II, *the trilateration* was developed after the launch of Sputnik. Observing the Doppler shift, the scientists understood that parameter refereed to the satellite signal gives information about the satellite time. In addition, the Kepler's law allowed the computation of the satellite ephemeris to determine accurate position on the Earth. Taking advantage from that observation, the Global Positioning System (GPS), the Russian Global'naya Navigatsionnaya Sputnikovaya Sistema (GLONASS) and the European Galileo have been developed (Hofmann-Wellenhof et al. [29]).

1.2.1 GLONASS

The studies on the Doppler satellite system Tsikada brought the Union of Soviet Socialist Republics (USSR) to the innovative military system GLONASS. Started just with military purpose, the Russian system has been extend to civil use but with severe restrictions. Positioned in the middle circular orbit, the GNSS satellites represents a valid alternative to GPS in high latitudes. At 19,100 km of altitude, with an inclination of 64.8 degree and a period of 11 hours and 15 minutes, the Russian global satellite navigation system transmit in Frequency Division Multiple Access (FDMA) on 15 channels. The standard precision signal and the high precision signal are modulated with Direct Sequence Spread Spectrum (DSSS) and Binary Phase Shift Keying (BPSK) modulation. By the end of 2020, the GLONASS is introducing the Code Division Multiple Access (CDMA) technique in addition to the

Figure 1.2: Glonass satellite [61]

already used FDMA method. The use of the same frequency slot for antipodal satellite resolves the interference effects of satellites in opposite position. The receiver on the Earth is not able to have both in visibility at the same time.

1.2.2 Galileo

The name of the famous Italian astronomer Galileo Galilei has been given to the European competitor of the Russian GLONASS and the GPS. The collective GALILEO system has the purpose to make Europe less dependent from Russia and USA. Developed from the European Union (EU) and the European Space Agency (ESA) , Galileo is providing high precision position system with a constellation of 30 satellites at 23.222 km of altitude. In the 2005, the ESA launched GIOVE (*Giove In-Orbit Validation Element*) test satellite, GIOVE-A. The International Telecommunication Union (ITU) used this aircraft to check the frequency allocation and the respect of the reservation requirements. Later, GIOVE-B introduced an more complex payload. Essentially, GALILEO conducts all the experiments using GIOVE A and GIOVE B using a receiver GETR. Successful results has been obtained and new study are conducted on this new system. The peculiarity is the BOC (*Binary Off-*
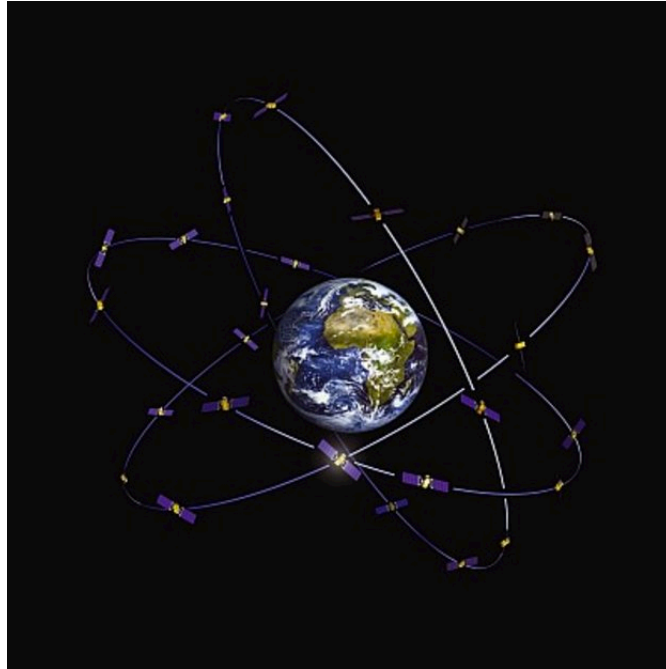
Figure 1.3: Galileo constellation [62]

set Carrier) modulation, which improves the tracking performance. The auto-correlation function of the BOC signal presents a mean lobe in the center and two small negative lobes on the sides. The mail peak reduces the multipath effects on the tracked signal.

1.2.3 GPS

The National Aeronautics and Space Administration (NASA) and the Department of Transportation(DOT) of the U.S.A. studied a time and positioning system in order to achieve global coverage, high accuracy (Kaplan [23]). At the basis of this new technology, there were satellites. In the 1960s, *Transit* and *Timation* satellites represent the first two projects. Both of them were abandoned cause their low performances and the Air Force presented the *System 621B*. The 621B proposed to innovations the elliptical orbit and the Pseudo-Random-Noise (PRN) modulation. These ideas were improved and developed by the Office of the Secretary of Defense (OSD) with the Navigation Satellite System program (DNSS) and the Navigation Satellite Executive Steering Group. From this time, the NAVSTAR

9

Global Positioning System or *GPS*'s provides a global coverage of time, position and velocity information to unlimited numbers of users on the Earth.

GPS constellation

In the 1993, the system achieved the operational capability of 24 satellites slipped in 4 satellites for each of the 6 elliptical orbits. Each orbit in nearly circular with an eccentricity of 0.01 and an inclination of 55°. With a period of 12 sidereal hours , the orbit has a semi-major axis of 26,560 km (El-Rabbany [11]). The GPS architecture consists of:

- *satellite side*

  - **the Space Segment**

  - **the Control Segment**

- *user side*

  - **User Segment**

The Space Segment

At the end of the 1970s until the beginning of the 1980s, the *Block I* of GPS satellites was launched with 10 operational satellites. In order to identify each satellites i, two characters are used: the first identifies the plane $(A, dots, F)$ and the second $(1, dots, 4)$ identifies the satellites on its orbit (Misra et al. [38]). Later, with the *Block II/II A* the constellation consisted of 24 satellites, distinguishing the civil users with the Coarse/Acquisition code (C/A code) and the military purpose with Precision code (PR code) [59]. The next generation was the *Block IIR/IIR M*, where 'R' stands for 'replenishment' (Misra et al. [38]), introducing the on-board clock monitoring, a two new military signals, a flexible power for military signals and Second civilian GPS signal (L2C) [59]. The *Block IIF*, where 'F' stands for 'follow-on' (Misra et al. [38]), brought an accurate clock and the civil signal L5
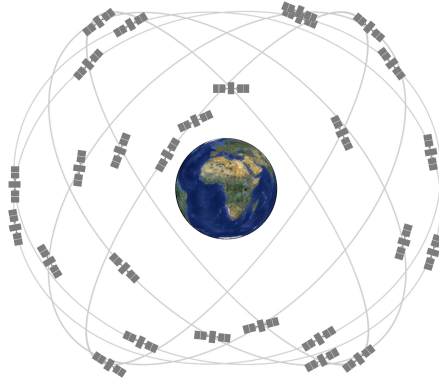
Figure 1.4: GPS constellation of 24 satellites [59]

for transportation safety [59]. Actually, the *Block III* is under development to introduce a fourth civilian GPS signal (L1C) for international interoperability [59].
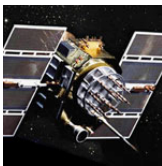
Figure 1.5: Block IIA [59]   Figure 1.6: Block IIR [59]   Figure 1.7: Block IIR (M) [59]   Figure 1.8: Block IIF [59]   Figure 1.9: Block IIiA [59]
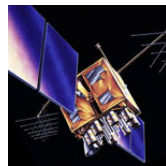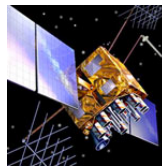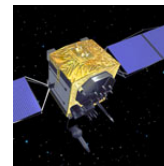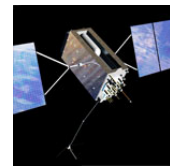
The Control Segment

The Control Segment consists of several GPS facilities on the Earth like [60]:

- Master Control Station (MCS): to monitor the health and the status of the satellite, sending commands to maneuvers the satellites if necessary (Misra [38]);

- Monitor Stations: to track the satellites updating the navigation message;

- Ground Antennas: to establish a communication with the satellites;

In addition, this segment predicts of the ephemeris and the clock parameters and maintains the GPS clock (Misra et al. [38]).

11
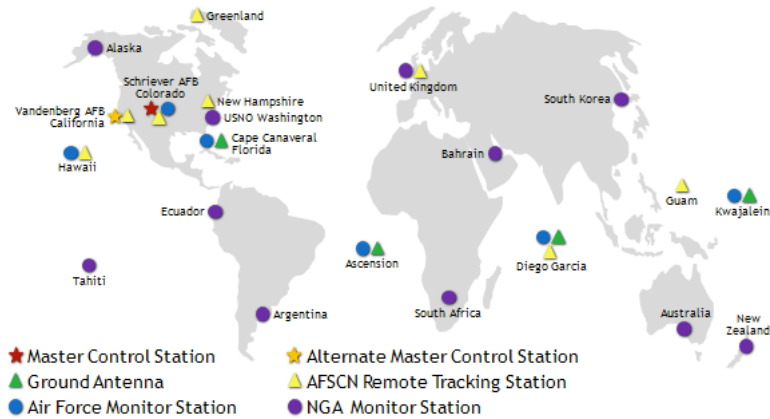
Figure 1.10: GPS Control Segment [60]

The User Segment

The User Segment is represented by the GPS receiver. In this years, several GPS receiver are in commerce, each of them to answer to the different requirements. The GPS receivers can be classified by their performance in terms of available parameters, accuracy, cost, aspect. The wide offers of receivers is due to the success of the GPS system for civil purposes as well as for military applications (Misra et al. [38]).

1.2.4 GPS Acquisition

The ability of the GNSS receiver to extract position, velocity and timing data consists in an architecture which combines the receiving data unit and the processing data unit. The information supplied by several satellites are collected by a right-hand circularly polarized (RHCP) antenna to be amplified by a low-noise amplifier (LNA), down converted to an intermediate frequency and digitalized. In order to calculate the position, velocity and timing data, the acquisition unit has to search and analyze the GPS signal.

The GPS acquisition represents a challenging stage for the receiver, and the time required to achieve the information represents a key point. In order to minimizing the time delay of the results, different methods have been used to perform the detection of the GPS signal.
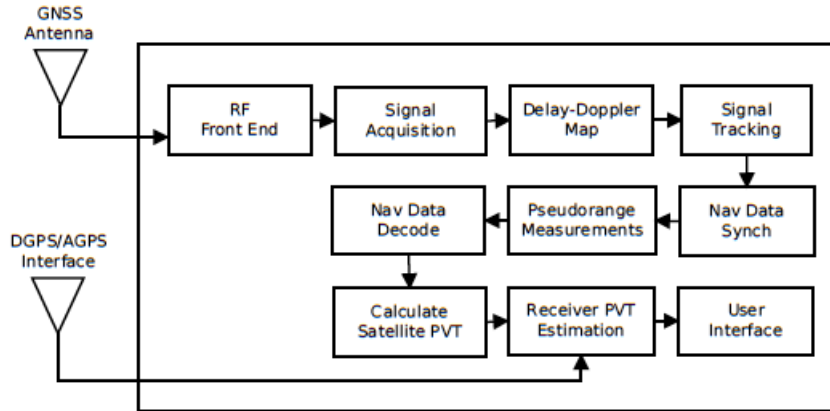
Figure 1.11: GPS receiver block diagram (Gleason et al. [21])

The first time when the receiver is turned on, the *cold start* represents an useful method. Due to a lack of a apriori knowledge, the receiver is forced to search the signal on the all 32 possible delays, causing a higher timing consume. Instead when the receiver owns previous estimations just of its last position, the almanac and the UTC time, a *warm search* is sufficient to complete the operation.

Cold GPS Serial Acquisition

The *cold start GPS acquisition* is an high time consumer acquisition algorithm. The received signal is (Misra et al. [38])

$$x^l(t) = PD^l(t-\tau)s^l(t-\tau)\cos(2\pi(f_{L1}+f_D)t+\phi) \tag{1.1}$$

where

- P is the signal power

- D^l are the navigation data

- $s^l(\cdot)$ is the the l satellite PRN code sequence

- τ is the delay

13

- f_{L1} is the carrier frequency L1 : 1575.72 MHz

- $f_{f_{dop}}$ is the Doppler frequency

- ϕ is the phase offset

The down-conversion of the received signal introduces a sufficient number of stages to respect the bandwidth properties. (Misra et al. [38])

$$x^l(t) = PD^l(t - \tau)s^l(t - \tau)\cos(2\pi(f_{IntFreq} + f_{dop})t + \phi) \qquad (1.2)$$

where

- P is the signal power

- D^l are the navigation data

- $s^l(\cdot)$ is the the l satellite PRN code sequence

- τ is the delay

- $f_{IntFreq}$ is the intermediate frequency 4.1304 MHz

- $f_{f_{dop}}$ is the Doppler frequency

- ϕ is the phase offset

The signal at the Intermediate frequency IF is multiplied by the C/A code replica $CA[n+m]$ for each nth sample and for all number of samples m^{th} that the C/A replica is phase shifted. Consequently, the components In-Phase and in Quadrature to be correlated and compared with a threshold to determine the presence or absence of a signal (Misra et al. [38]).

The filtered signal is multiplied by the In-Phase and In-Quadrature signal's components, respectively.

$$In\ phase\ reference\ signal = 2cos(2\pi(f_{IntFreq} + \hat{f_{dop}})t + \phi) \qquad (1.3)$$
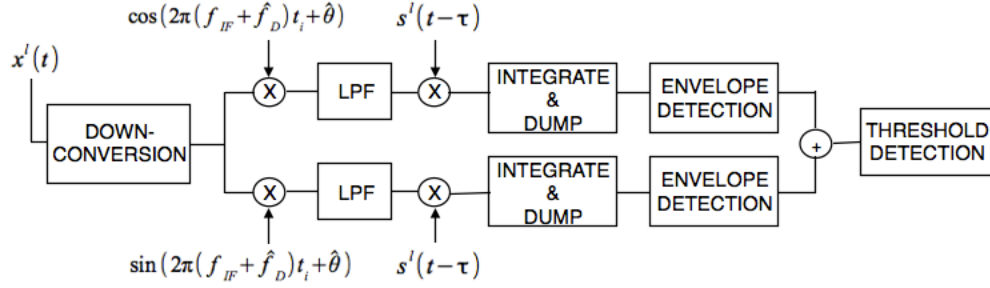
Figure 1.12: Serial Cold Acquisition

$$In\ quadrature\ reference\ signal = -2sin(2\pi(f_{IntFreq} + \hat{f_{dop}})t + \phi) \qquad (1.4)$$

obtaing the component in phase and the component in quadrature of the filtered signal:

$$\sqrt{A}D(t-\tau)x(t-\tau)cos(2\pi\Delta f_{dop}t + \Delta\phi) \qquad (1.5)$$

$$\sqrt{A}D(t-\tau)x(t-\tau)sin(2\pi\Delta f_{dop}t + \Delta\phi) \qquad (1.6)$$

The result of this operation is a signal function of two differential factors, independent from each other:

- the difference between the Doppler frequency and the estimated Doppler frequency

$$\Delta f_{dop} = f_{dop} - \hat{f_{dop}} \qquad (1.7)$$

- the difference between the input phase and the estimated phase

$$\Delta\phi = \delta\phi - \hat{\phi} \qquad (1.8)$$

The importance of the In-Phase and In In-Quadrature process is in the ability of the receiver to discriminate a closing range from an opening range. In the first case, the Doppler fre-

15

quency is positive because the satellites is moving forward the receiver. In the second case, the Doppler is negative because the satellite is going further from the receiver. In addition, the In-Phase and In-Quadrature correlator process the I/Q signals obtaining

$$S_{In-Phase}(\Delta\tau,\Delta f_{dop},\delta\phi) = \frac{\sqrt{AD}}{T_{coe}} \int_0^{T_{coe}} x(t-\tau)x(t-\hat{\tau})cos(2\pi\Delta f_{dop}t+\Delta\phi)dt \qquad (1.9)$$

$$S_{In-Quad}(\Delta\tau,\Delta f_{dop},\delta\phi) = \frac{\sqrt{AD}}{T_{coe}} \int_0^{T_{coe}} x(t-\tau)x(t-\hat{\tau})sin(2\pi\Delta f_{dop}t+\Delta\phi)dt \qquad (1.10)$$

where

- $\Delta e_\tau = \delta - \hat{\tau}$ is the code delay error.

- $T_{coe} <$ duration of a data bit is the coherent averaging time

Combining $S_{In-Phase}$ and $S_{In-Quad}$ in a complex signal S

$$S = S_{In-Phase} + S_{In-Quad} = \sqrt{AD}e^{j\Delta\phi}R(\Delta\tau,\Delta\phi) \qquad (1.11)$$

where $R(\Delta\tau,\Delta\phi)$ is called *ambiguity function* and is related to the correlation function.

$$R(\Delta\tau,\Delta\phi) = \frac{1}{T_{coe}} \int_0^{T_{coe}} x(t-\tau)x(t-\hat{\tau}e^{j2\phi\Delta f_{dop}t}dt \qquad (1.12)$$

The parameter $(\Delta\tau,\Delta\phi)$ are estimated computing :

$$|S|^2 = S_{In-Phase}^2 + S_{In-Quad}^2 = \rho|R|^2 \qquad (1.13)$$

Cold GPS FFT Acquisition

The GPS Acquisition based on the Fast Fourier Transform (FFT) algorithm is usually used in modern receiver due to its reduced computation time of the millisecond order (Van Nee et al. [49]). In order to achieve fast and better performance, this technique performs the

16
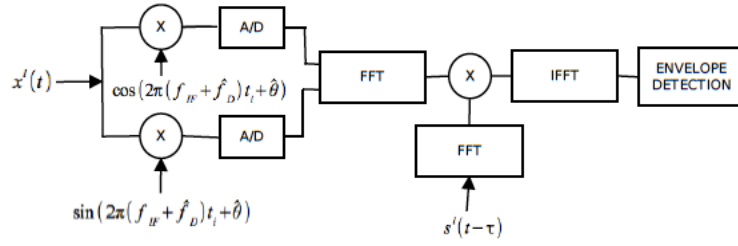
Figure 1.13: Cold GPS FFT Acquisition

FFT of the complex signal:

$$FFT(I(\Delta\tau, \Delta f_{dop}, \delta\phi) + jQ(\Delta\tau, \Delta f_{dop}, \delta\phi)) \tag{1.14}$$

where

- $I(\Delta\tau, \Delta f_{dop}, \delta\phi)$ is the In-Phase component of the filtered down-converted received signal

$$I(\Delta\tau, \Delta f_{dop}, \delta\phi) = \sqrt{A}D(t - \tau)x(t - \tau)cos(2\pi\Delta f_{dop}t + \Delta\phi) \tag{1.15}$$

- $Q(\Delta\tau, \Delta f_{dop}, \delta\phi)$ is the in quadrature component of the filtered down-converted received signal

$$Q(\Delta\tau, \Delta f_{dop}, \delta\phi) = \sqrt{A}D(t - \tau)x(t - \tau)sin(2\pi\Delta f_{dop}t + \Delta\phi) \tag{1.16}$$

Reminding that a multiplication in the frequency domain corresponds to a convolution in the time domain, it is possible to obtain the correlation signal from a multiplication in the frequency domain. Performing the Inverse Fast Fourier Transform (IFFT) of the multiplication of the conjugate of the FFT signal by the FFTs of all the 32 C/A codes $s^l(\cdot)$ the correlation signal is obtained.

Warm Search

While the GPS receiver is working, the position and time parameter are stored in its memory. If the device is turned off and then turned on again, it estimates the position and the time using the values recorded in the memory. Knowing the previous satellites position, time and almanac, the receiver computes the actual position and time of the satellites. In this way, the elaboration is reduced, otherwise the receiver needs to analyze the time-of-week and the ephemeris before to estimate the position (Van Diggelen [51]).

1.2.5   GPS C/A code

The IS-GPS-200D (*Navstar*) defines the exactly structure of the GPS signal. That signal is formed by three main parts:

- **Carrier frequency** : each GPS satellite uses two transmitted frequencies $f_{L1} = 1575.42MHz$ and $f_{L2} = 1227.60MHz$

- **Ranging code** : in order to provide service, at each satellites have been associated a Pseudo-Random-Noise code (PRN code). The orthogonal property of the PRN sequences allows the communication of many satellites at the same frequency without any risk of interference.

- **Navigation data** : the high demanding precision of satellites system requires additional information to prevent possible errors. The 20 ms Navigation binary sequence is transmitted every 50 ms and received after 12.5 ms. The Navigation data contain the satellites health status, the almanac, the clock bias parameters and the ephemeris, these last two repeated every thirty seconds.
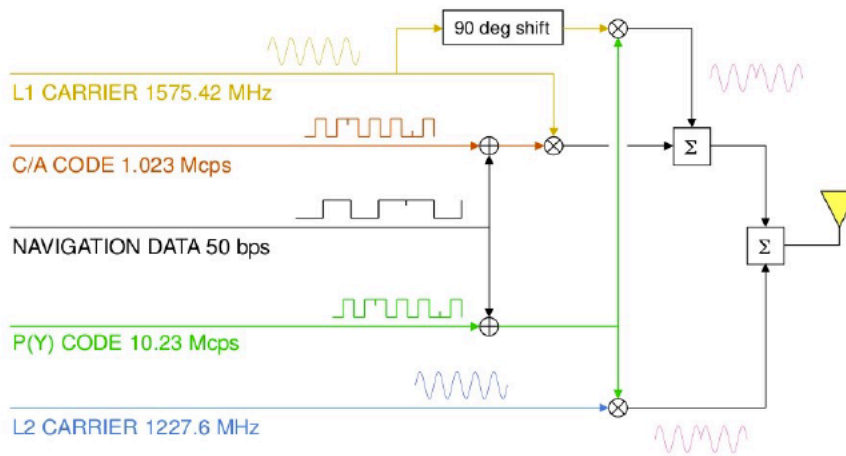
Figure 1.14: GPS Signals Generation (Larson [32])

PRN sequence

The Standard Positioning Service (SPS) and Precise Positioning Service (PPS) possible services, provided with a satellite communication, are associated to two different sequences. The PPS has designed for military use or for users equipped with a PPS receivers, instead the SPS has civil purposes, which require less accuracy than the military ones (DoD [9]). The SPS service is offered as C/A code, and transmitted on L1 frequency. Instead the PPS service is a precision, encrypted code P(Y)-codes transmitted on L1 and L2 frequencies. The incapability of the direct acquisition of the PPS code required a coarse code, the C/A code. This sequence is 1023 bits (*chips*) long, with a duration of $1\mu sec$ and repeated every *msec*. The chips are characterized by a *chip rate* of 1.023 MHz or 1.023 Mcps. The chips can be seen as the bits multiplied for the speed of the light. In fact, the *chip width* or wavelength of each chip is

$$chip\ width = 1\mu sec * 299792458m/sec \approx 300m \tag{1.17}$$

Register	Initial State	Polynomial
C/A code G1	1111111111	$1 + x^3 + x^{10}$
C/A code G2	1111111111	$1 + x^2 + x^6 + x^8 + x^9 + x^{10}$
P code X1A	001001001000	$1 + x^6 + x^8 + x^{11} + x^{11}$
P code X1B	010101010100	$1 + x^1 + x^2 + x^5 + x^8 + x^9 + x^{10} + x^{11} + x^{12}$
P code X2A	100100100101	$1 + x^1 + x^3 + x^4 + x^5 + x^7 + x^8 + x^9 + x^{10} + x^{11} + x^{12}$
P code X2B	010101010100	$1 + x^2 + x^4 + x^4 + x^8 + x^9 + x^{12}$

Figure 1.15: GPS Code Generator Polynomials and Initial States

A more precise code ($\approx 10^4 chips$ is used for the P(Y) sequence, the PRN code. The higher *chip rate* 10.23 Mcps and the smaller *chip width* 30 m corresponds to more accurate range measurements.

PRN Code Generation

The GPS C/A code is recursively generated shifting two 10-bit registers G1 and G2. The Coarse/Acquisition sequence is a Gold sequence. This type of code is used mainly in a broadcasting environment in Telecommunications and GPS, where more devices are transmitting at the same time the same frequency. The Gold code is a sequence of $2^n - 1$ with an auto-correlation factor close to 1 and a cross-correlation factor approximately 0. In the GPS application, the Gold code is generated using the following *Generator Polynomials*

For the 10-bits shift register G1, the taps 3 and 10 are summed modulo-2 at each clock event. Instead for the 10-bits shift register G2, the sum modulo-2 uses taps 2,3,6,8,9,10. Both the registers are initialized to all 1.

The set of C/A codes is a set of 32 possible sequences, each of them with a length of 1023 bits with a chipping rate of 1.023 MHz and a repetition period of 1 millisecond. Each C/A sequence is computed multiplying the 1023-bit sequence obtained from the shift register G1 and the delayed version of the 1023-bit sequence obtained shifting the 10-bit

POLYNOMIAL G1:

$$1 + X^3 + X^{10}$$
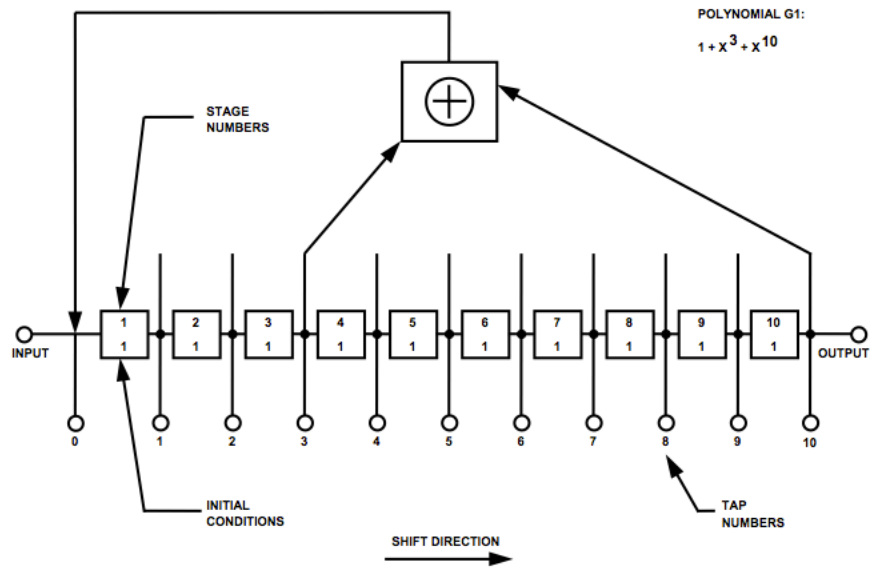
Figure 1.16: G1 Shift Register Generator (Navstar [30])

POLYNOMIAL G2:

$$1 + X^2 + X^3 + X^6 + X^8 + X^9 + X^{10}$$
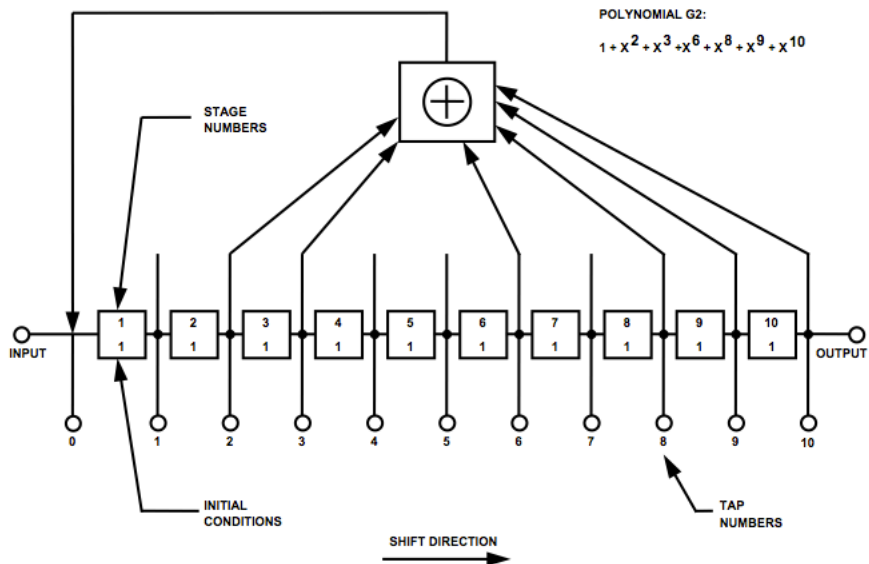
Figure 1.17: G2 Shift Register Generator (Navstar [30])

register G2. The set of 32 C/A sequences is generated to allow 32 different satellites to transmit at the same frequency and at the same time without interfere each other.

PRN sequence properties

The PRN code is a sequence of +1 and -1 with two main properties (Misra et al. [38])

- **nearly orthogonality**

  If we consider 2 satellites p and t, the sum of the term by term product of the 2 C/A codes x^p and x^t, relatively shifted to each other is nearly zero.

  $$\sum_{k=0}^{1022} x_{(k)}^{(p)} \cdot x_{(k+m)}^{(t)} \approx 0 \tag{1.18}$$

  $$\begin{cases} \text{for all } m \text{ and for } p \neq t \\ x^{(\cdot)}(1023+n) = x^{(\cdot)}(m) \end{cases}$$

  The C/A codes are *nearly uncorrelated* to each other. This allows to use different satellites at the same time and with the same frequency without any risk of interfering.

- **nearly auto-uncorrelated**

  The PRN sequence is *nearly auto-uncorrelated*. The sum of the term-by term product of on C/A code x^p with its n delayed version is approximately zero. At *0* delay corresponds a huge peak of the *auto-correlation* function.

  $$\sum_{k=0}^{1022} x_{(k)}^{(p)} \cdot x_{(k+m)}^{(p)} \approx 0 \tag{1.19}$$

  $$\text{for all } |m| \geq 1$$

These two properties are analyses in the acquisition and in the tracking of the GPS signal.

PRN Number	C/A Code Tap Selection	C/A code Delay	First 10 C/A Chips(octal)	P-code Delay	First 12 P Chips(octal)
1	2·6	5	1440	1	4444
2	3·7	6	1620	2	4000
3	4·6	7	1710	3	4222
4	5·8	8	1744	4	4333
5	1·9	17	1133	5	4377
6	2·6	18	1455	6	4355
7	1·8	139	1131	7	4344
8	2·9	140	1454	8	4340
9	3·10	141	1626	9	4342
10	2·3	251	1504	10	4343
11	3·4	252	1642	11	4343
12	5·6	254	1750	12	4343
13	6·7	255	1764	13	4343
14	7·8	256	1772	14	4343
15	8·9	257	1775	15	4343
16	9·10	258	1776	16	4343
17	1·4	469	1156	17	4343
18	2·5	470	1467	18	4343
19	3·6	471	1633	19	4343
20	4·7	472	1715	20	4343

Figure 1.18: Code-Phase Assignments C/A code

PRN Number	C/A Code Tap Selection	C/A code Delay	First 10 C/A Chips(octal)	P-code Delay	First 12 P Chips(octal)
21	5·8	473	1746	21	4343
22	6·9	474	1743	22	4343
23	1·3	509	1063	23	4343
24	4·6	512	1706	24	4343
25	5·7	513	1743	25	4343
26	6·8	514	1761	26	4343
27	7·9	515	1770	27	4343
28	8·10	516	1774	28	4343
29	1·6	859	1127	29	4343
30	2·7	860	1453	30	4343
31	3·8	861	1625	31	4343
32	4·9	862	1712	32	4343
33[1]	5·10	863	1745	33	4343
34[1]	4·10	950	1713	34	4343
35[1]	1·7	947	1134	35	4343
36[1]	2·8	948	1456	36	4343
37[1]	4·10	950	1713	37	4343

[1]PRN codes 33,34,35,36,37 are reserved

Figure 1.19: Code-Phase Assignments C/A code
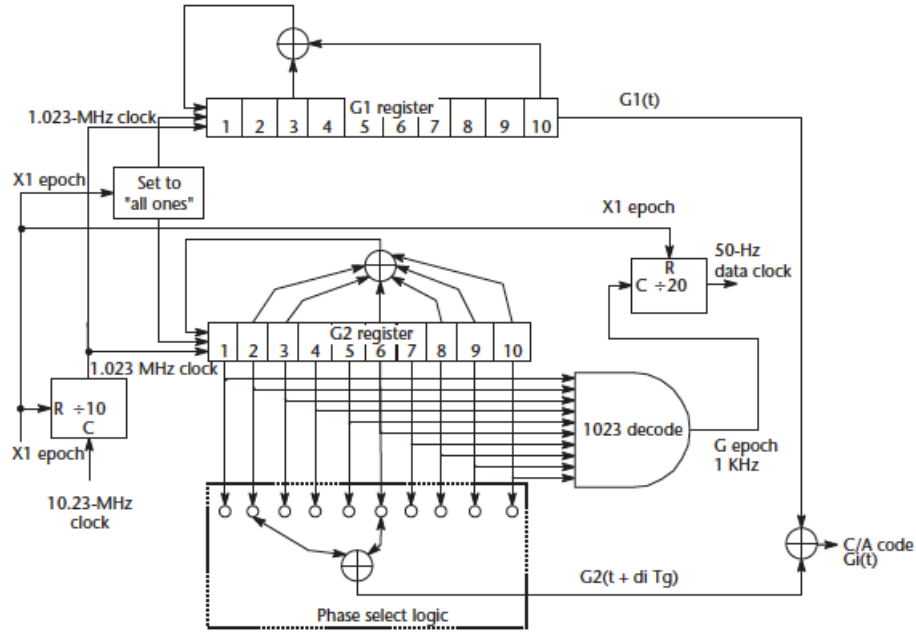
Figure 1.20: Example of a C/A code generator (Kaplan [23])

Auto-correlation Function and Power Spectrum

The auto-correlation function is a measure of the similarity of a signal with its delayed version in the time domain. Considering that a C/A sequence can be seen as a known and period rectangular pulse train of amplitude 1 and -1, in order to analyses the auto-correlation properties of the C/A code it is important to deep on a rectangular pulse and a random binary code (Kaplan [23]). In the time domain, the general equation for a rectangular pulse with amplitude $A_r t$ and bandwidth T_c is

$$x_{rt}(t) = \begin{cases} A_{rt} & \frac{T_c}{2} \leq t \geq \frac{T_c}{2} \\ 0 & otherwise \end{cases} \tag{1.20}$$
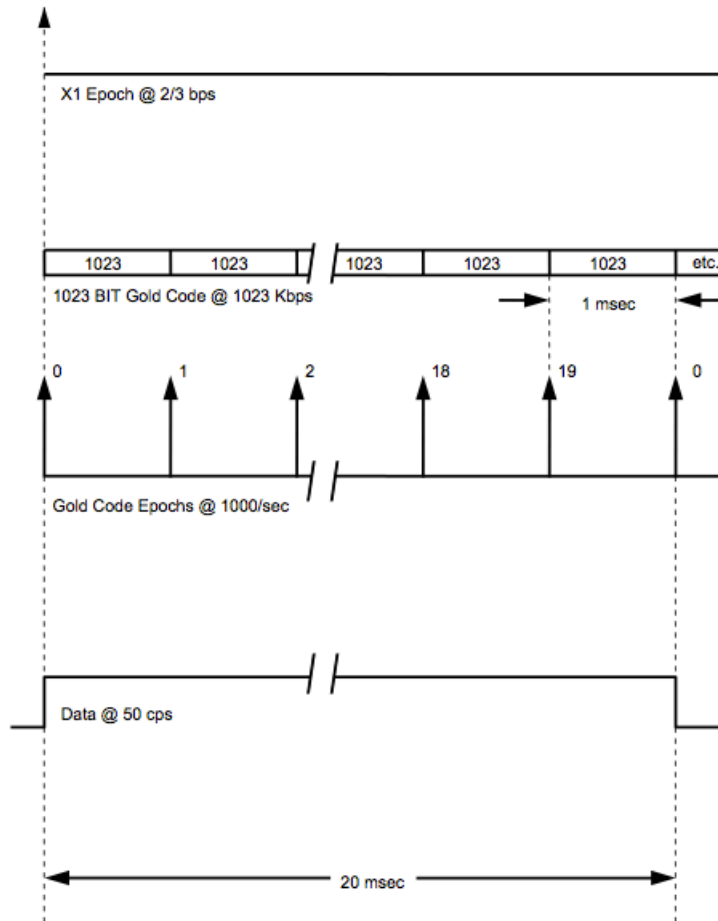
Figure 1.21: C/A code timing relationship (Navstar [30])

In the frequency domain, the rectangular pulse corresponds to a sinc function with a maximum amplitude AT_c at $\omega = 0$ and and amplitude equal to zero in all the multiples of $\pm\frac{2\pi}{T_c}$.

$$
\begin{aligned}
X_{rt}(\omega) &= A_{rt}T_c\left\{\frac{sin\frac{\omega T_c}{2}}{\frac{\omega T_c}{2}}\right\} \\
&= A_{rt}T_c sinc(fT_c) where\begin{cases} \omega = 2\pi f\left[\frac{rad}{sec}\right] \\ f = frequency[Hz] \end{cases}
\end{aligned}
\tag{1.21}
$$

In a communication system, the signal processing on the transmitted signal is introduced to make the signal more robust to the interference and the deleterious effects introduced from the communication environment, the communication channel and the communication system. In order to conduct a successful communication, and receive the right information with less distortions as possible, the signal processing theory has introduced specific parameters as the auto-correlation, the cross-correlation functions and the power density function. These functions are measures of the of the signal respect to itself and respect to the other signal transmitted at the same time, or at the same frequency or using the same encoding technique. For analog system, the auto-correlation function of an analog signal $x(t)$ can be defined as (Proakis et al. [39]):

$$
R_x(\tau) = \int\limits_{-\infty}^{+\infty} x(t)x^*(t-\tau)dt
\tag{1.22}
$$

where

- τ is the positive time delay between the signal $x_{rt}(t)$ and its replica $x_{rt}(t-\tau)$

- * is the symbol for the conjugation operation

The auto-correlation function assumes its maximum value when time delay τ is 0. In this case, the auto-correlation corresponds to the energy of the non-periodic signal, or to the

power of the periodic signal (Proakis et al. [39])

$$\varepsilon_x = \int\limits_{-\infty}^{+\infty} |x(t)|^2 \, dt = R_x(0)$$

$$P_x = \lim_{T_c \to \infty} \frac{1}{T_c} \int\limits_{-\frac{T_c}{2}}^{+\frac{T_c}{2}} |x(t)|^2 \, dt = R_x(0)$$

(1.23)

The auto-correlation of the rectangular impulse (Figure 1.22) is a triangular pulse with amplitude $A^2 T_c$ and bandwidth $2T_c$:

$$R_{x_{rt}}(\tau) = \int\limits_{-\infty}^{+\infty} x_{rt}(t)x_{rt}^*(t-\tau)dt = \begin{cases} A_{rt}^2 T_c \left(1 - \frac{|\tau|}{T_c}\right) & for \ |\tau| \le T_c \\ \\ 0 & otherwise \end{cases}$$

(1.24)

The mathematical property of the maximum amplitude at $\tau = 0$ is important in a scenario where the signal is transmitted at the same frequency that at different time. If the auto-correlation is low between the signal and its replica corresponds to a lack of interfere between the two waveform even though they have the same shapes and the same frequency. In the frequency domain, the Fourier Transform of the auto-correlation function is the Power Spectral Density Function (PSD) (Proakis et al. [39]):

$$S_x(\omega) = FT(R_x(\tau))$$

(1.25)

Fort the rectangular pulse (Figure 1.22), the *PSD* $S_{rt}(\omega)$ is the absolute value of a sinc function of amplitude $A_{rt}^2 T_c$: (Kaplan [23])

$$S_{rt}(\omega) = A_{rt}^2 T_c^2 \left(\frac{sin\frac{\omega T_c}{2}}{\frac{\omega T_c}{2}} \right)^2 = A_{rt}^2 T_c^2 sinc^2 \frac{\omega T_c}{2}$$

(1.26)

essentially the *PSD* is the absolute value of the squared Fourier Transform (Kaplan [23])

$$S_{rt}(\omega) = |X_{rt}(\omega)|^2$$

(1.27)

This relation can be used to compute the PSD of a random binary code, which is a sequence of rectangular impulses of amplitude $\pm A_{rbc}$ and a chip period T_c (Kaplan [23]). The auto-correlation function and the PSD differ of a scale factor T_c from the ones of the rectangular pulse. Tha auto-correlation is:

$$R_{x_{rbc}}(\tau) = \int_{-\infty}^{+\infty} x_{rbc}(t)x_{rbc}^*(t-\tau)dt = \begin{cases} A_{rbc}^2\left(1-\frac{|\tau|}{T_c}\right) & for\ |\tau| \le T_c \\ 0 & otherwise \end{cases} \tag{1.28}$$

and the PSD is

$$S_{rbc}(\omega) = A_{rbc}^2 T_c \left(\frac{sin\frac{\omega T_c}{2}}{\frac{\omega T_c}{2}}\right)^2 = A_{rbc}^2 T_c sinc^2 \frac{\omega T_c}{2} \tag{1.29}$$

The peculiarity of this code is to be uncorrelated with its delayed replica, the auto-correlation assumed the maximum value 1 just when the random binary code is correlated with itself not delayed. After these considerations, let focus on the GPS code. The *Pseudo-Random-Noise* code $x_{PRN}(t)$ is a sequence of period rectangular impulse of amplitude $\pm A_{PRN}$, each pulse of chip period T_c. The auto-correlation function for a code length M is (Kaplan [23]):

$$R_{x_{PRN}}(\tau) = \frac{1}{MT_c} \int_0^{MT_c} x_{PRN}(t)x_{PRN}(t-\tau)dt \tag{1.30}$$

Reminding that the auto-correlation function for a rectangular pulse is a triangular with pick at zero-delay. The auto-correlation of a periodic sequence of rectangular impulse is a specular series of triangular functions of amplitude $\pm A_{x_{PRN}}$ and period MT_c. Mathematically, it can be expressed as the convolution of the triangular function and the train of the Dirac-δ impulses:

$$R_{x_{PRN}}(\tau) = \frac{-A_{PRN}^2}{M} + \frac{M+1}{M}R_{x_{PRN}}(\tau) \otimes \sum_{n=-\infty}^{\infty} \delta(\tau+nMT_c) \tag{1.31}$$
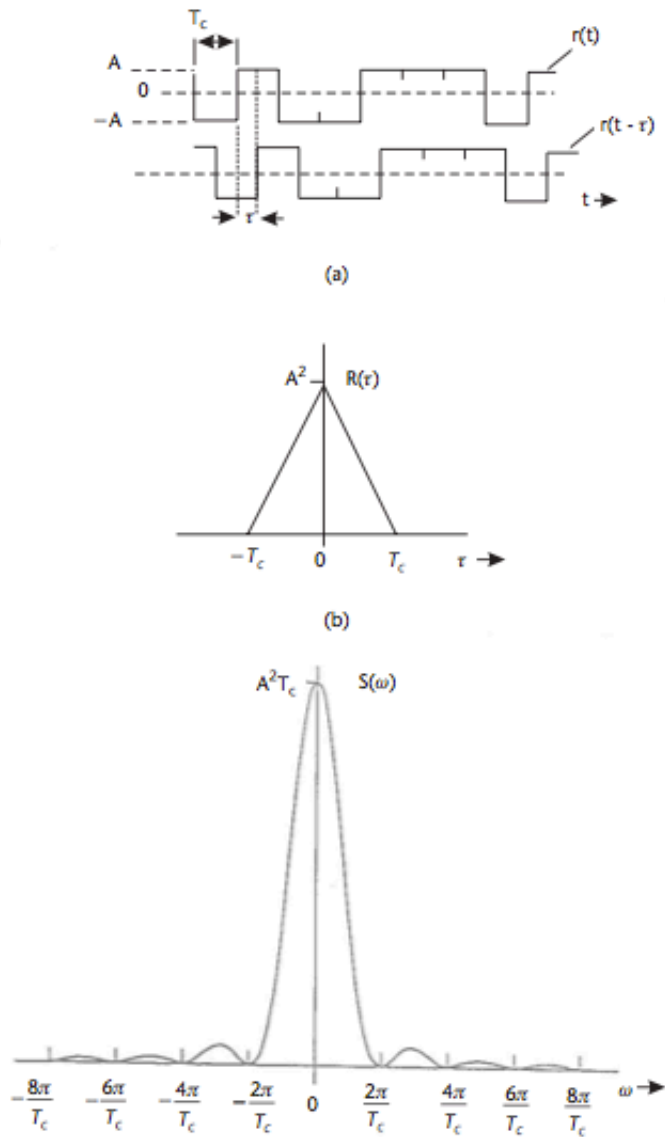
Figure 1.22: a)example of random binary code b)auto-correlation c) PSD (Kaplan [23])
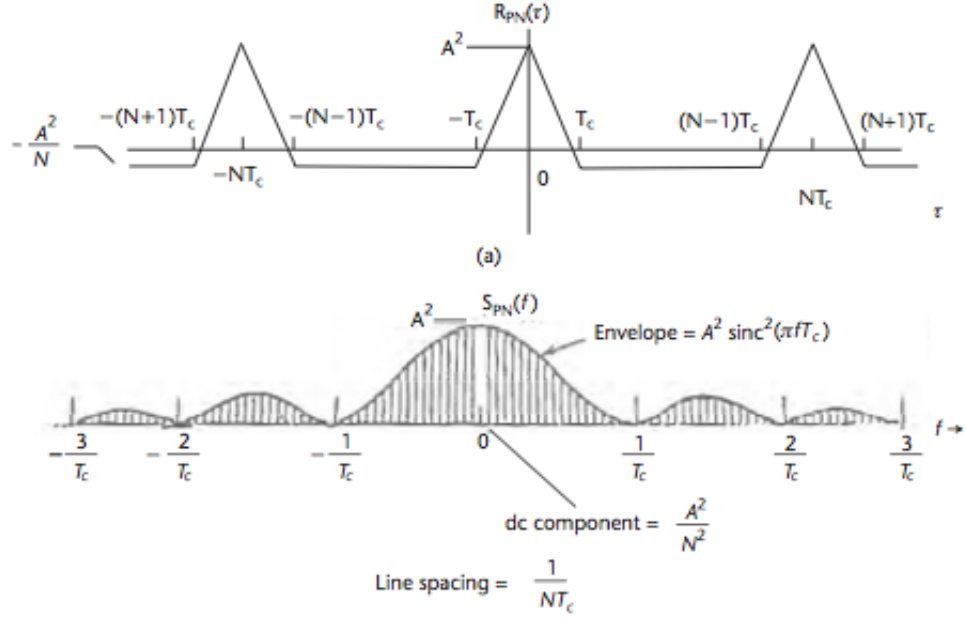
Figure 1.23: a)auto-correlation function of PRN code b)PSD (Kaplan [23])

and the PSD is

$$
\begin{aligned}
S_{x_{PRN}}(\omega) &= |R_{x_{PRN}}(\tau)|^2 \\
&= \frac{A_{PRN}^2}{M^2}\left[\delta(\omega) + \sum_{\substack{n=-\infty \\ \neq 0}}^{\infty}(M+1)sinc^2\left(\frac{n\pi}{M}\right)\delta\left(\omega + \frac{2n\pi}{MT_c}\right)\right]
\end{aligned}
\tag{1.32}
$$

$$
for\ n = \pm1, \pm2, \pm3, \ldots
$$

The $2^m - 1$ C/A sequence x_{GPS}, generated by two shifted registers G1 and G2 of $m = 10$ bits, has auto-correlation function (Kaplan [23])

$$
R_{C/A}(\tau) = \frac{1}{1,023 T_c} \int_{t=0}^{t=1023} x_{GPS}^k(t) x_{GPS}^k(t - \tau) dt
\tag{1.33}
$$

where:

- $k = 1, 2, \cdots, 32$ is the C/A sequences index

- x_{GPS}^k is the C/A sequence related to the delay k

31
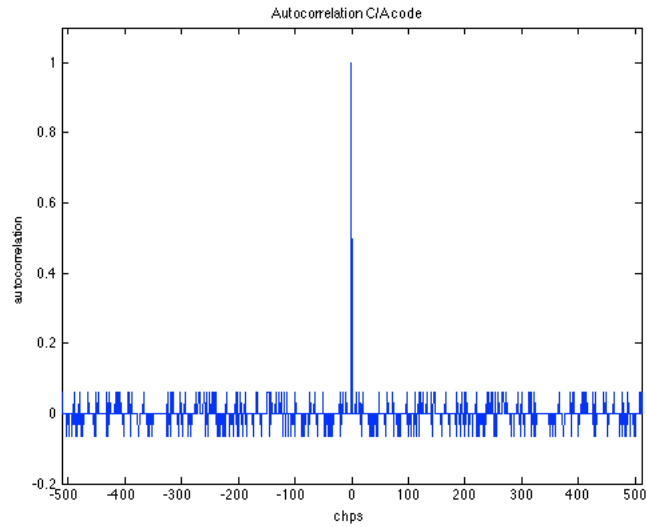
Figure 1.24: Auto-correlation function of C/A code

- T_c *is the chipping period* 977.5*nsec for a C/A code*

- τ *is the delay in the auto-correlation function*

The obtained plots confirm what asserted before. The C/A code is maximum correlated with itself in multiples of the period *1 ms* (*nearly auto-correlated*), and it is uncorrelated with the other C/A codes (*nearly orthogonality*).
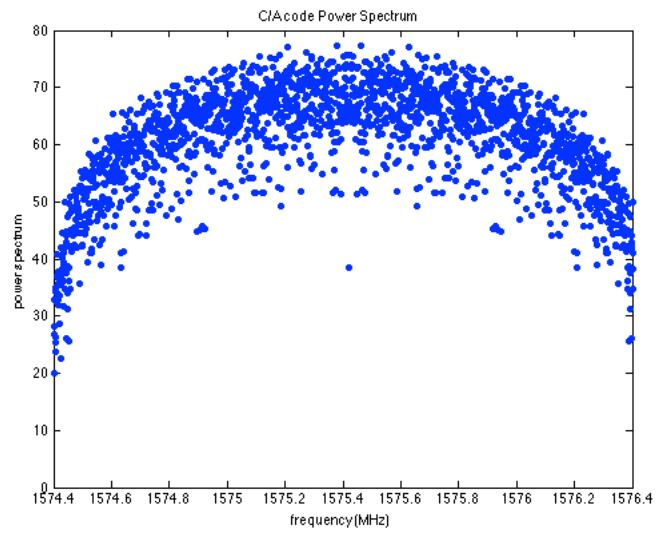
Figure 1.25: PSD of C/A code

Chapter 2

Field Programmable Gate Array

2.1 Introduction

The Field-Programmable Gate Array (FPGA) is a integrated circuit re-configurable and re-programmable after the manufacturing. The FPGA contains programmable logic components called logic elements (LEs) who are interconnected by re-configurable interconnects to implement the desired function. Thank to the reconfiguration of the interconnections and the re-programmability of the LEs, complex combinational functions can be performed as well as simple logical gate but a good knowledge of the implemented algorithm, the software and the hardware are required .

2.2 FPGA architecture

The FPGA is a multi-levels architecture similar to the Programmable Logic Devices (PLD), but with better performance and efficiency. Several components are contained in a FPGA like:

- Multiplexer

- Configurable embedded SRAM
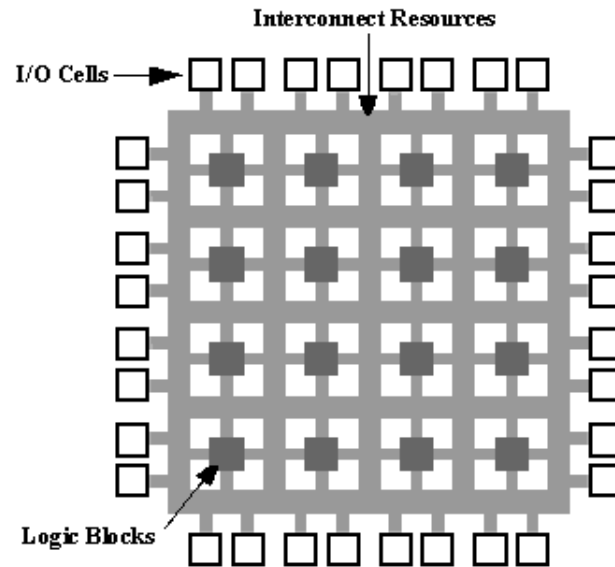
Figure 2.1: FPGA architecture (Xilinx [63])

- Transistor pairs

- Look-Up Tables (LUTs)

- High-Speed I/Os

- NAND-XOR gates

- High-Speed Transceivers

- AND-OR structures.

One of the main problem of the design on FPGA is the limit of the resource. In order to achieve good performance, it is necessary to take care of the area occupancy and time delay. Through flessibility and the re-programmability of the FPGA is possible to optimize the design reducing the risk of low efficiency. A strategy that can be used with that purpose is the use of Look Up Tables (LUTs) to implement (Francis [12])

- logical gates

35

- counters, multipliers, signal generator, coder, encoder, etc

- complex mathematical computations

. As it is possible to notice, the LEs and the interconnections between them play an important roll. There are several configurations of the interconnections, each of them is used based on the requirements of the design. The interconnections can be classified as (Lanzagorta et al. [31])

- Nearest Neightbor : interconnections between logic blocks and the closest logic blocks (timing delay linearly proportional to the distance)

- Segmented : more complex, depending on LUTs, connection blocks and switch boxes (increasing routing flexibility)

- Hierarchical : hierarchical connection of logic blocks in segmented structure
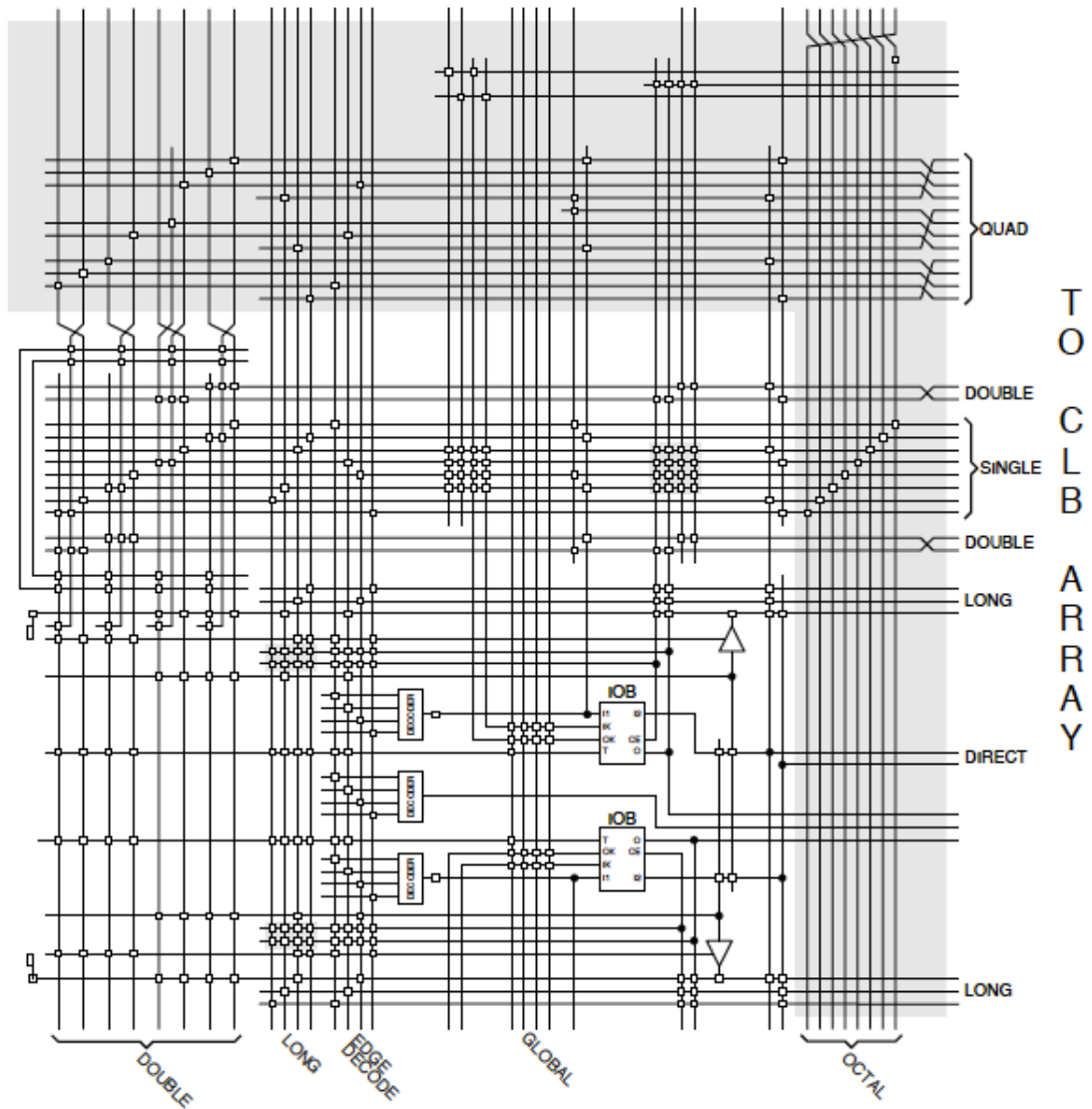
Figure 2.2: Programmable Interconnect Details in XC4000E and XC4000X Series FPGA (Xilinx [56])

37

The process of reconfiguration of the FPGA, can be summarized in 6 main step (Lanzagorta et al. [31]):

- **Functional Description**: the programmer describes the desired algorithm through a *Hardware Description Language (HDL)*, such as VHDL or Verilog

- **Logic Synthesis**: The description of the algorithm is converted into a circuit with interconnected logic gates.

- **Technology Mapping**: the architecture of the circuit is built following the interconnected logic gates.

- **Placement**:the architecture is mapped in the FPGA logic gates.

- **Routing**: the software optimize the interconnections configuration in order fit the FPGA

- **Bit-stream Generation**: a binary file of the circuit is created to be downloaded on the FPGA

2.3   VHDL: the pros and cons

The VHSIC Hardware Description Language (VHDL), where *VHSIC* stands for *Very High Speed Integrated Circuits*, is an hardware programming language used for electronic chips. VHDL is a strongly typed language, no case sensitive based on ADA and Pascal. This programming languages, which uses IEEE standards, is algorithmic deficient, not allowing the intermixing, or operation of variables, with different types and requiring several line of codes to implement simple arithmetic expressions (Botros [3]). On the other side, VHDL is a data-flow language portable and multipurpose, periodically revised to follow the industry trends. The choice to design the "GPS Acquisitions in VHDL on FPGA" has been made considering the peculiarity of this programming languages and of the FPGA. Design such

algorithm in VHDL means to be able to create and use complex data types, even though not defined in the libraries, taking advantage of the wealth of constructs. Programming in VHDL allows to have a perfect idea and control of the operations on the programmed devices. Due to its high-performances in the implementation of complex algorithm, VHDL is the language used to achieve the GPS Acquisition design on the FPGA. The FPGA is a technology, which offers high computation performances in short processing time. Therefore, designing the GPS Acquisition in VHDL on FPGA will reduce significantly the computation's timing delay compared to other implementation on Matlab, or C++.

2.4   Xilinx-Virtex FPGAs

The Xilinx-Virtex 6 FPGA family has been chosen to develop this work. The Virtex-6 family presents low power consumption, more processing power and updated interfaces compered to its predecessors Virtex-4 and Virtex-5.

The Virtex-6 as most of the Xilinx FPGAs respects a name convection. The chosen FPGA for this thesis has been Virtex-6 XC6VLX240T FF1156 -2 with 240,000 logic cells (Xilinx [54]), divided in block of 6 cells each to form the slice or in block of 2 slices to form 1 CLB (*Configurable Logic Block*). The Virtex-5 family presents the same organization of logic cells. Instead of the Virtex-4 family is configured with slices of 2 logic cells each and CLBs of 4 slices. A higher numbers of CLBs corresponds to a slower system, but also to a more flexible architecture (Xilinx [52], [53], [54]).

In addition to the increasing logic cells of the Virtex-6, this device presents also a clock rate of 600 MHz due to the increasing switching rate of the shrinking transistors. Indeed, the logic cells' size change from 90nm to 65nm to 40 nm comparing the Virtex-4, Virtex-5 and Virtex-6 families, respectively. The different architectures structures results in a clock rate of 500 MHZ for the Virtex-4 and in a clock rate of 550 MHz in Virtex-5. This increasing operational rate provides better performances in the dedicated DSP slices (*Digital Signal*

Virtex devices available in a 35 mm x 35 mm BGA package			
Resource	Virtex-4*	Virtex-5*	Virtex-6*
Logic Cells	41K – 152K	46K – 156K	128K – 476K
Slices**	18K – 68K	7K – 24K	20K – 74K
CLBs	4608 – 16896	3600 – 12160	10000 – 37200
Block RAM (kb)	1728 – 6768	2160 – 8784	9504 – 38304
DSP Slices	64 – 512	48 – 640	480 – 2016
Serial Transceivers	0 – 20	12 – 16	20
SelectIO	448 – 768	480 – 640	600

* Virtex-4 FX, LX, and SX devices; Virtex-5 FXT, LXT and SXT devices; Virtex-6 LXT and SXT devices
** Virtex-4 Slices actually require 2.25 Logic Cells and Virtex-5 and Virtex-6 Slices actually require 6.4 Logic Cells

Figure 2.3: Architectures comparison: Virtex-4 Family, Virtex-5 Family, Virtex-6 Family (Xilinx [64])

Processor), as the multiply-accumulator (Xilinx [64]).

For what concerns the Block RAM, the Virtex-6 has a capability of 38 Mbits, a significant improvements compared to the 7 Mbits, 8 Mbits of the Virtex-4 and Virtex-5. The Virtex-6 is equipped of serial GTX and GTH transceivers interfaces, with an ability to transfer data at rates of Gbits/sec, really helpful in high bandwidth systems.

Chapter 3

C/A code and Digital Design

The design of the Coarse Acquisition code on an FPGA represents an significant improvement in terms of performance and efficiency of a satellite system. For this reason, the design of the GPS Acquisition has been started with the design of the C/A sequence for the all 32 possible delays on FPGA.

The search of the GPS signal on all the 32 possible delay is used in the Cold search, when the GPS receiver does not have any information to calculate the its position. For each delay is computed a C/A code, and to each C/A code is associated a satellite. As shown in the 3.1, the generation of each C/A code can be summarize in 6 steps:
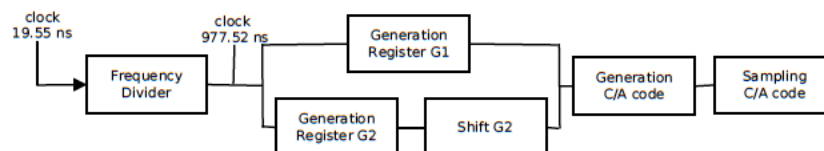
1. Frequency Divider

2. Generation Register G1

Figure 3.1: Block diagram of the C/A code design

3. Generation Register G2

4. Shift Register G2

5. Generation C/A code

6. Sampling of the C/A code

3.1 Frequency Divider

The Frequency divider is a component which allows to reduce the input frequency of a specific scale factor to achieve the desired frequency. In the case of the C/A code, the frequency of the code is 1.023MHz, instead the internal frequency of the system is 50 MHz, so it is necessary to reduce the system frequency of a factor

$$Scale\ Factor = \frac{input\ frequency}{output\ frequency} = \frac{50*10^6}{1.023*10^6} = 49$$

where

- *50 MHz=clock* $\frac{1}{50*10^6} = 20ns$

- *1.023 MHz=clock* $\frac{1}{1.023*10^6} = 97.752ns$

The Frequency divider generates an output frequency of 1.023 MHz each 50 cycles. The Frequency divider can be represented like a counter that counts from 0 to the *Scale Factor-1* generating a triggered clock high, and when the number is higher than the *Scale Factor*, the counter is re-set and the process restarts and the triggered clock is set to low (Figure 3.2).

The output of the Frequency Divider is used as clock of the next blocks.
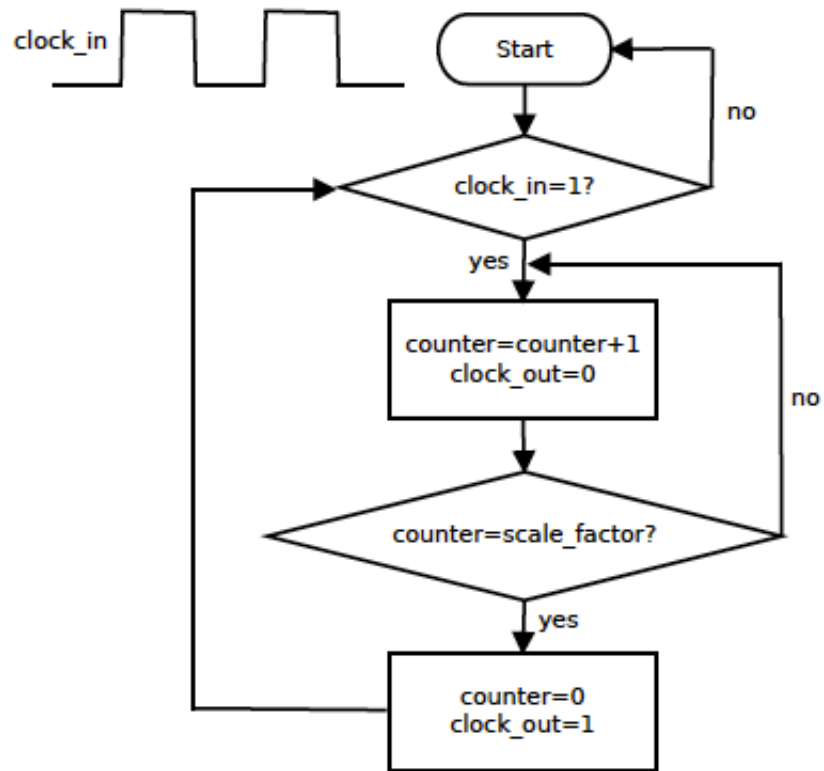
Figure 3.2: Flow diagram: Frequency Divider
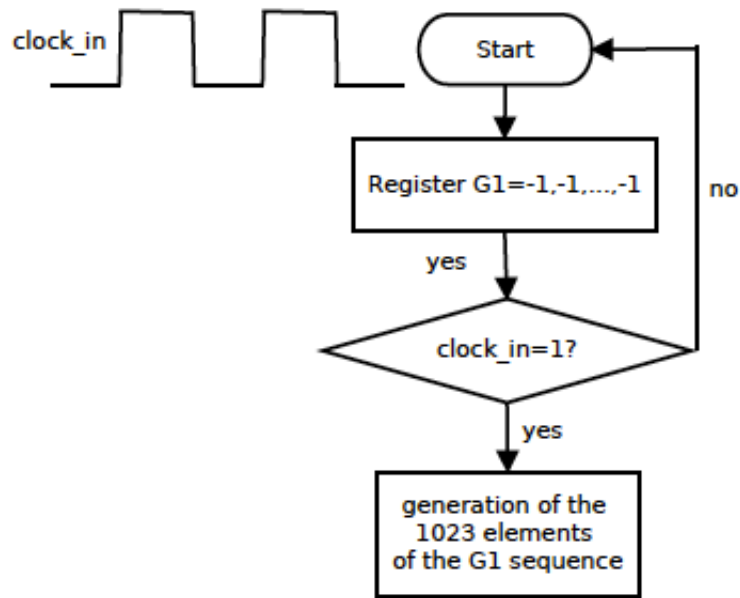
Figure 3.3: Flow diagram: Generation Register G1

3.2 Generation Register G1

Using the clock generated with the Frequency Divider, the G1 Shift Register Generation is performed. A integer register *Register G1* of 10 elements is declared, and each element is to -1. At each rising edge of the clock, the element in the 10th position and the element in the 3th position are added *modulo-2* ($\oplus$), as showed in 1.16, to generate a vector of 1023 elements. Considering that the *Register G1* is a vector of integer, the elements are multiplied (Figure 3.3).
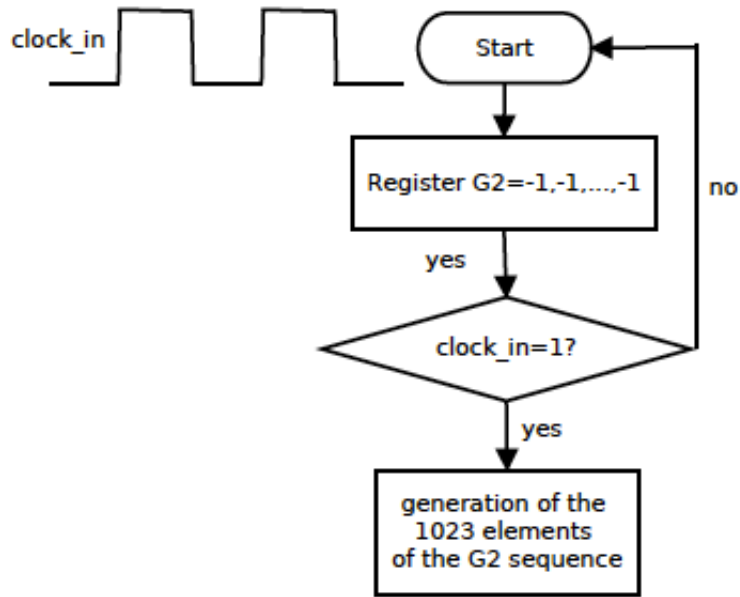
Figure 3.4: Flow diagram: Generation Register G2

3.3 Generation Register G2

As did for the G2 Shift Register Generation, the clock generated with the Frequency Divider is used as clock of this block. A integer register *Register G2* of 10 elements is declared, and each element is setted to -1. At each rising edge of the clock, the element in the $2^{nd}, 3^{th}, 6^{th}, 8^{th}, 9^{th}$ position and the element in the 10th position are added *modulo-2* ($\oplus$), as showed in 1.17, to generate a vector of 1023 elements. Considering that the *Register G2* is a vector of integer, the elements are multiplied (Figure 3.4).

3.4 Shift Register G2

The output of the G2 Shift Register Generation block needs to be shifted by 32 different delay, one for each satellites, before to be multiplied for the output of the G1 Shift Register Generation block. The results of this operation is a matrix of 32 rows of 1023 elements,
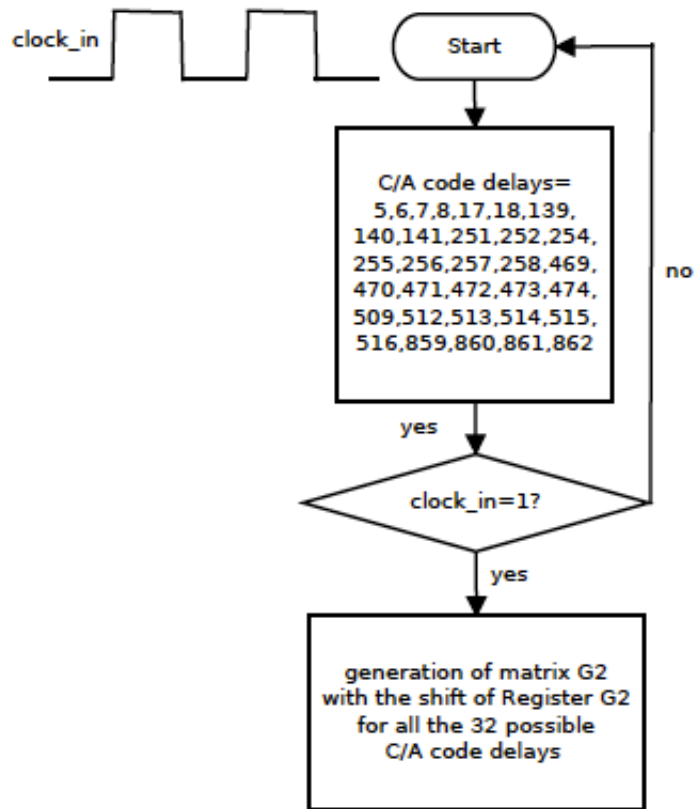
Figure 3.5: Flow diagram: Generation of the Matrix G2

one row for each delay (Figure 3.5).

3.5   Generation C/A code

The generation of the C/A code is done simply multiplying the output of the block *Generation Register G1* by each row of the output matrix of the block *Shift Register G2* (Figure 3.6).

The output is a matrix of 32 rows of 1023 elements, which assumes integer values between (-1,1), as shown in 3.7. In order to say that this is a set of C/A codes, it is necessary to prove that the generated sequences respect the C/A code properties as explained in *Chapter 2*.
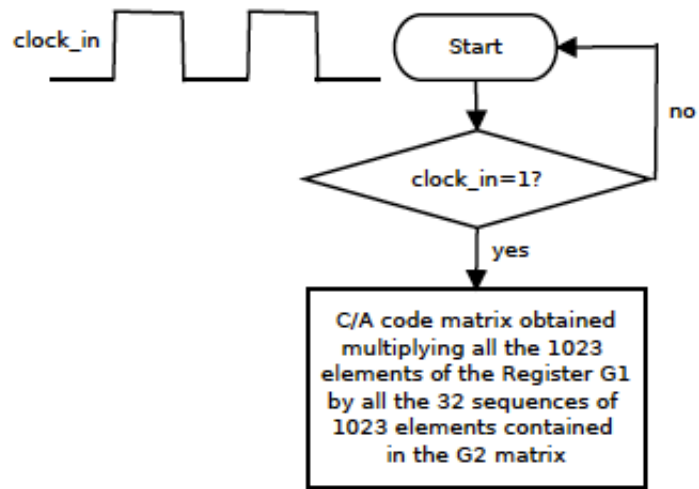
Figure 3.6: Flow diagram: Generation of the 32 possible C/A codes
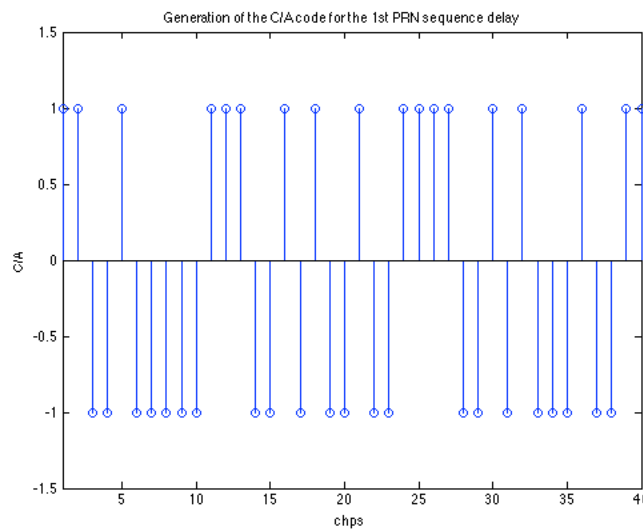
Figure 3.7: 1st C/A sequence generated in VHDL
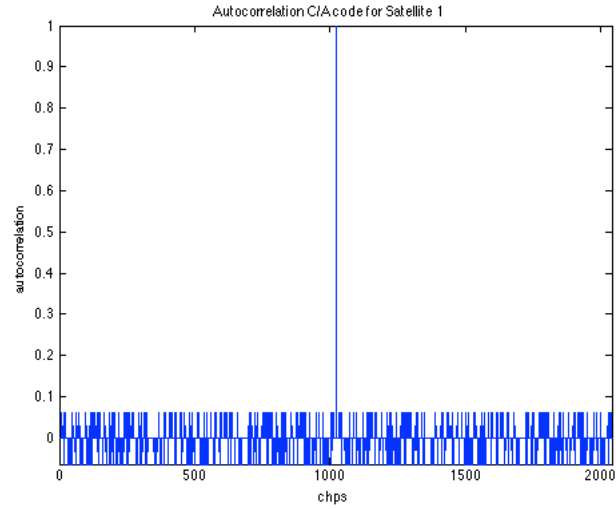
Figure 3.8: Autocorrelation function of the 1st C/A sequence generated in VHDL

As shown in 3.8 and in 3.9 for the 1st and the 2^{ns} sequences, the generated C/A code sequences are **nearly orthogonal** and **nearly uncorrelated**. In addition, the powers of the generated sequences are all the absolute value of a **sinc-function**, as in 3.10 for the 1st sequence.
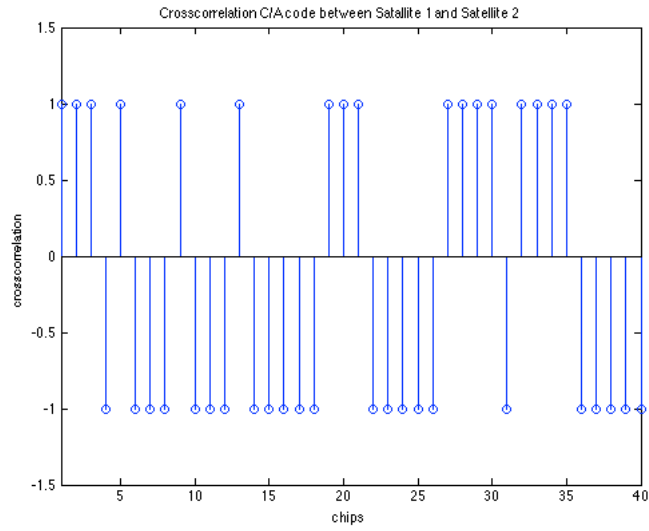
Figure 3.9: Cross-correlation function of the 1st and the 2nd C/A sequences generated in VHDL
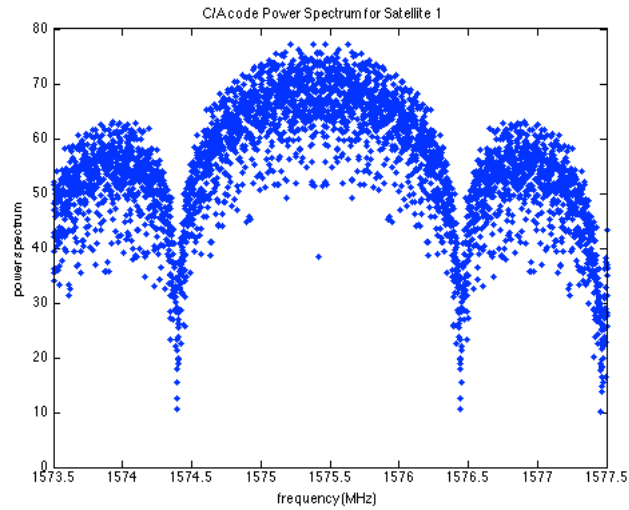
Figure 3.10: Power-Spectral Density *PSD* function of the 1s C/A sequences generated in VHDL

49
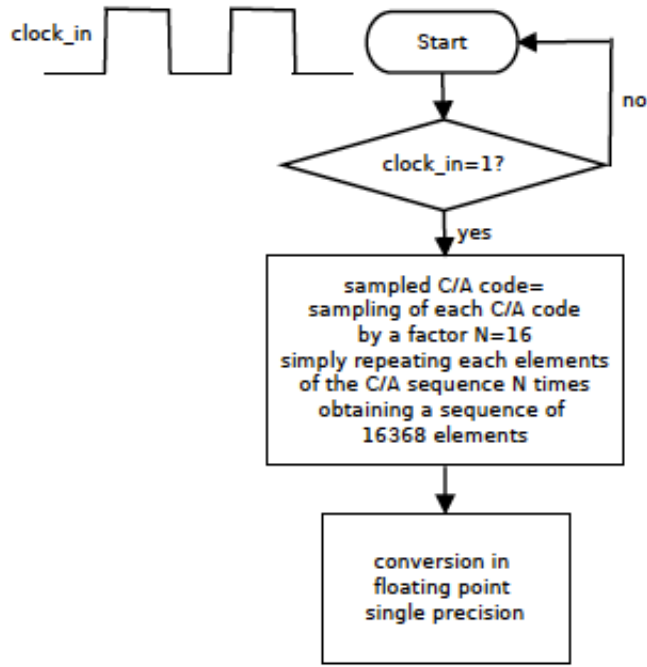
Figure 3.11: Flow diagram: Sampling of the 32 possible C/A codes

3.6 Sampling of the C/A code

The last block performs the sampling of each C/A sequence for 1 ms of data (Figure 3.11). This means that each sequence is sampled for a factor

$$N = \left\lfloor \frac{Sampling\,Frequency}{Code\,Frequency} \right\rfloor = \left\lfloor \frac{16.3676 * 10^6}{1.023 * 10^6} \right\rfloor = 16 \qquad (3.1)$$

where $\lfloor \rfloor$ represents an operation of rounding down to the next smallest integer.

The sampling process can be seen as the repetition of each elements of the sequence for N times, obtaining a final sequence of M elements.

$$M = \left\lfloor \frac{Sampling\,Frequency}{Code\,Frequency} \right\rfloor * 1023 = \left\lfloor \frac{16.3676 * 10^6}{1.023 * 10^6} \right\rfloor * 1023 \qquad (3.2)$$

Chapter 4

Digital Acquisition

In this work, the main purpose was to reduce the time delay and the processing time. Considering that every time a unit has been recalled, it increases the time delay and the processing time, the design of the GPS Acquisition has been thought using a clock of 50 MHz and the parallel of 32 block units, one for each C/A code.

4.1 FFT Cold Acquisition

The FFT Cold Acquisition has been designed with a pipelined configuration, one branch for each of the 32 possible satellite channels. Each branch of this design contains the cascade
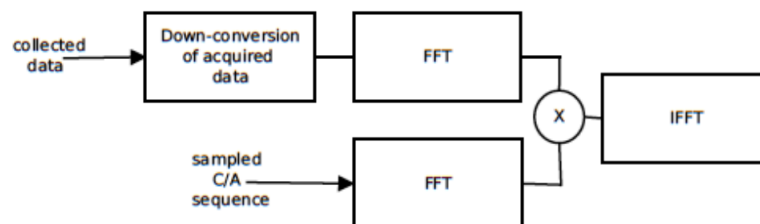
Figure 4.1: Design of the FFT Acquisition of the GPS signal for a single C/A sequence: block diagram

of the following components:

- Down-conversion of acquired data

- FFT

- IFFT

- Envelope detector

4.1.1 Down-conversion of acquired data

The down-conversion of the acquired data performs the multiplication of the acquired data and the trigonometric function:

- $sin(2\pi f_{IntFreq}t)$

- $cos(2\pi f_{IntFreq}t)$

where

- $f_{IntFreq}$ is the intermediate frequency 4.1304 MHz

- t is the time vector

In order to simplify the operations, these trigonometric functions have been approximated to a rectangular waveform as illustrated in the flow diagram Figure 4.2
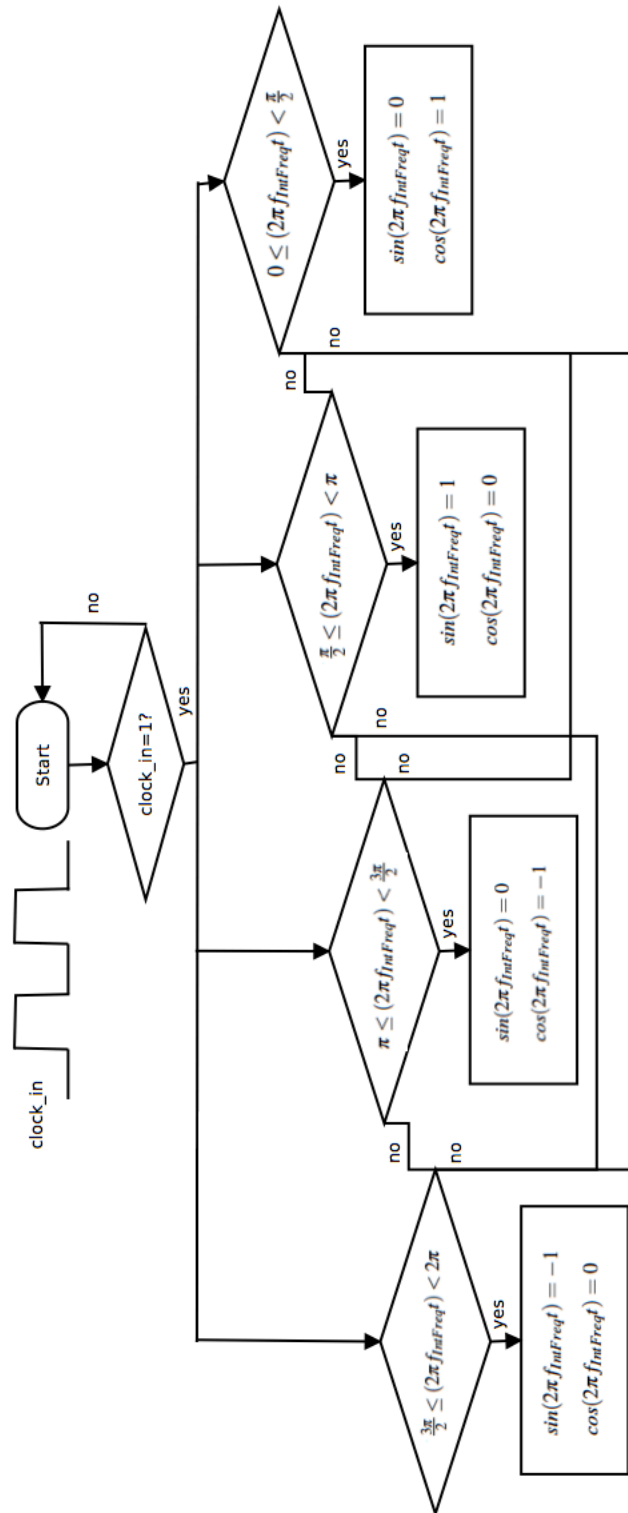
Figure 4.2: Flow diagram: Generation of the Loop Up Tables in the Down-Conversion Unit
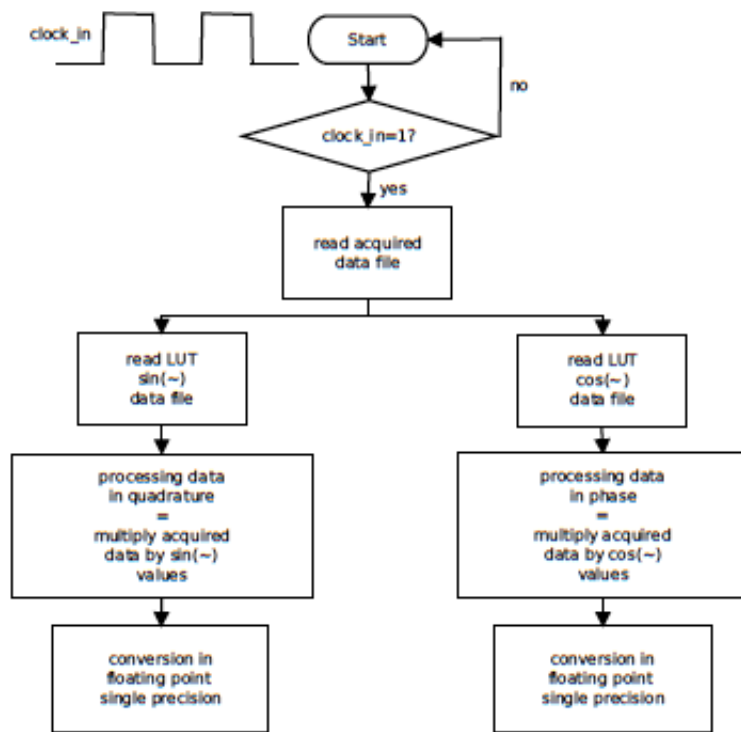
Figure 4.3: Flow diagram: Down-Conversion Unit

Using this approximation, two Look-Up-Table have been created in Matlab, one with all the values of the $sin(\cdot)$ and one with all the values of the $cos(\cdot)$. These LUT has been loaded into the VHDL-design and multiplied by the acquired data to perform the down-conversion(Figure 4.3).

4.1.2 FFT of down-converted signal

The FFT unit represents the focal unit in this algorithm. In this project, the Xilinx LogicIP Core has been used to perform the FFT on 16384 points. After the generation of the FFT Xilinx IP Core v.7.1 (Xilinx [55]), the down-converted signal has been converted in floating point in single precision. The real and the imaginary part of the converted data have be
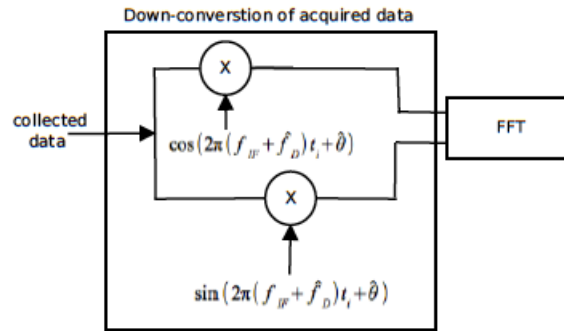
Figure 4.4: Design of the down-conversion of collected data: block diagram

setted as input of the FFT, obtaining a sequence of complex floating point data in single precision as output, consequently converted into integer (Figure 4.5).

In order to obtain a Delay Doppler Map, all the calculations have been done considering a range of Doppler frequency.

4.1.3 FFT of C/A code

The same FFT unit generated for the down-converted signal has been used to elaborate each of the 32 C/A sequences. Each C/A code has been converted into floating point in single precision IEEE 754 to be processed with the FFT unit. The output data have been converted into integer (Figure 4.6).

4.1.4 IFFT

In order to detect the GPS signal, the FFT acquired data has been multiplied for each of the 32 C/A code and processed with the IFFT algorithm on 16384 points. The results of the multiplication have been converted into floating point in single precision IEEE 754 and setted as input of the IFFT unit, generated using the FFT Xilinx LogicIP Core v.7.1 (Xilinx
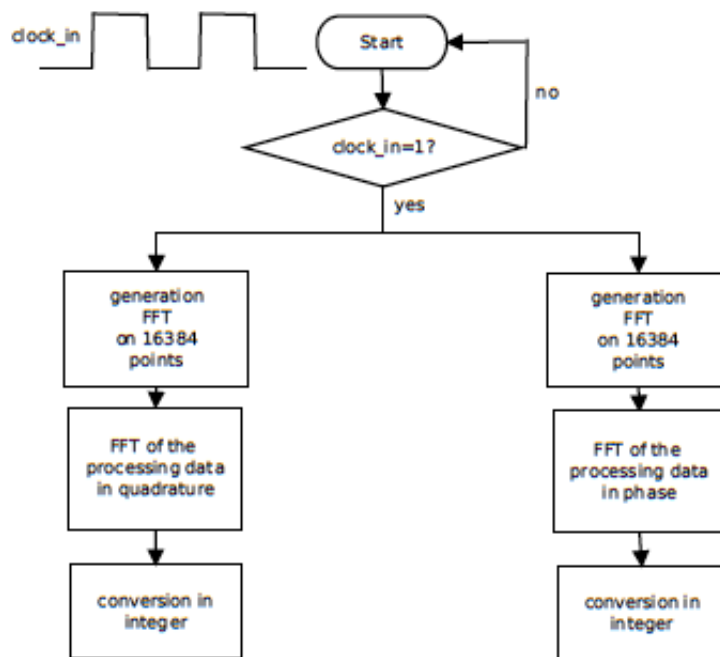
Figure 4.5: Flow diagram: FFT of down-converted data
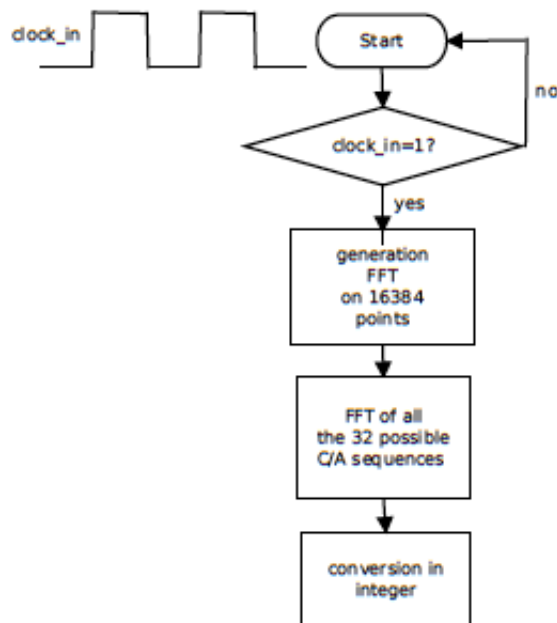
Figure 4.6: Flow diagram: FFT of all the 32 possible C/A codes

[55]). The results of this elaboration have been converted into integer (Figure 4.7).

4.1.5 Envelope detector

An Envelope Detector is in cascade with the IFFT Unit to select the IFFT output sequences with a magnitude's peak at least twice the average noise's value. These sequences correspond to the GPS signal candidates (Figure 4.9).

4.1.6 Final Envelope Detector

In order to plot the Delay-Doppler Map of the GPS signal, a final envelope detector has been introduced to select the GPS signal candidate with the highest magnitude's peak. The obtained DDM is stored and plotted as function of the delay chips and the Doppler frequency's range.

4.2 Serial Cold Acquisition

The Serial Acquisition has been designed following the same principle used for the FFT Acquisition design. A pipelined design is able to respect the requirement of a low timing delay. For that reason, the serial acquisition is done using a pipelined architecture with 32 branch, one for each of the 32 possible channels. Each branch contains:

- Split in-phase and in-quadrature processing

- Integration and Dump

- Envelope Detector
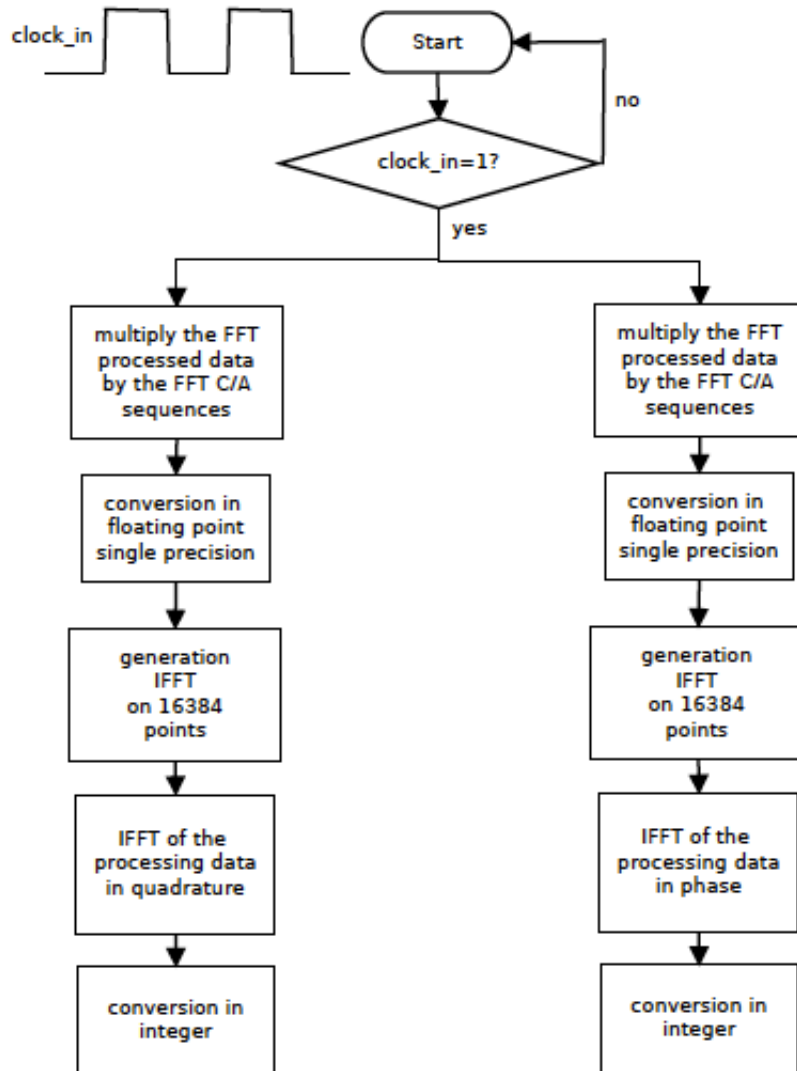
Figure 4.7: Flow diagram: IFFT of the processed data

Figure 4.8: Complete design of the FFT Acquisition of the GPS signal for the 32 C/A sequence: block diagram
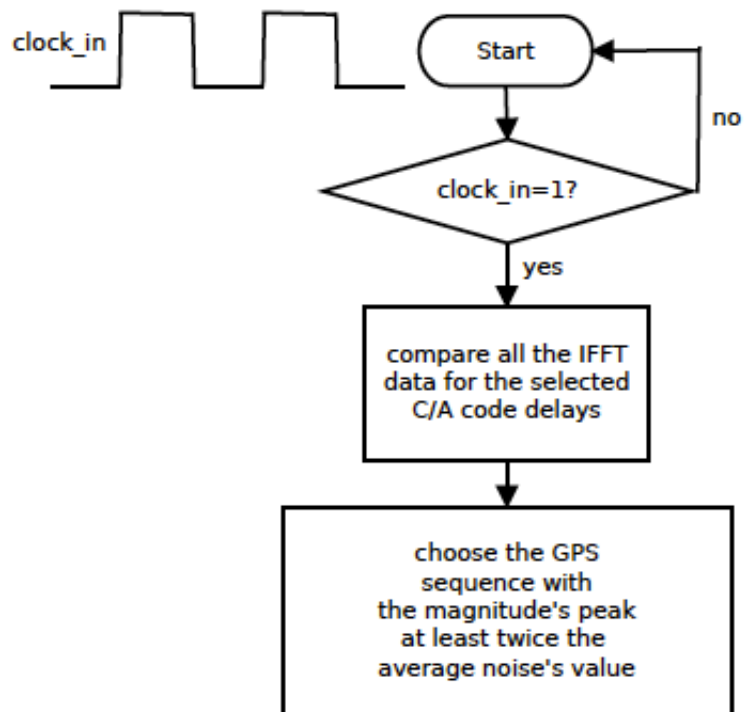
Figure 4.9: Flow diagram: Envelope Detector to select the best GPS signal
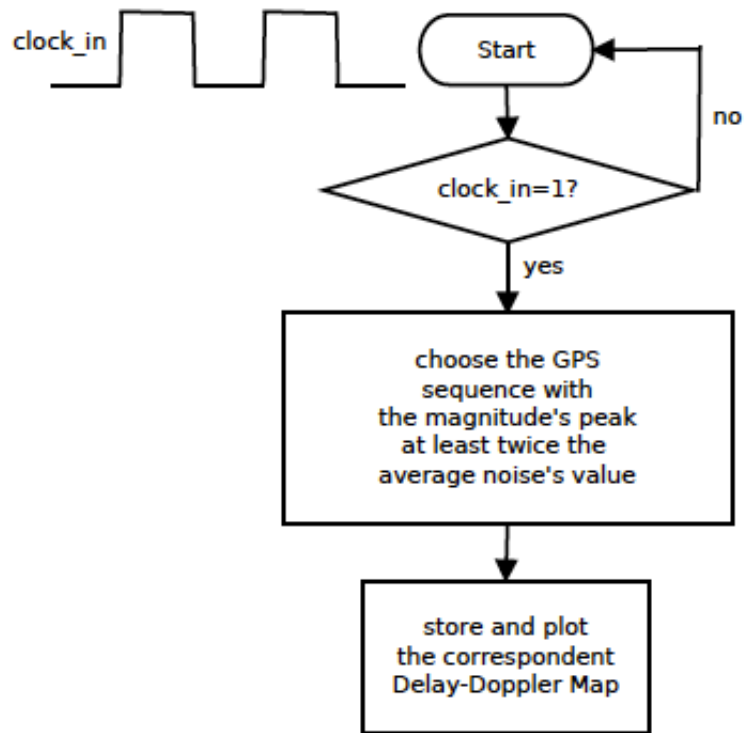
Figure 4.10: Flow diagram: Final Envelope Detector to select DDM with the best GPS signal
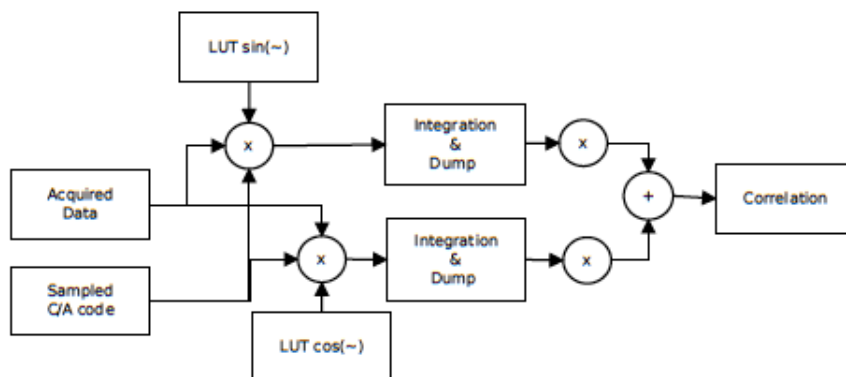
Figure 4.11: Design of the Serial Acquisition of the GPS signal for a single C/A sequence: block diagram
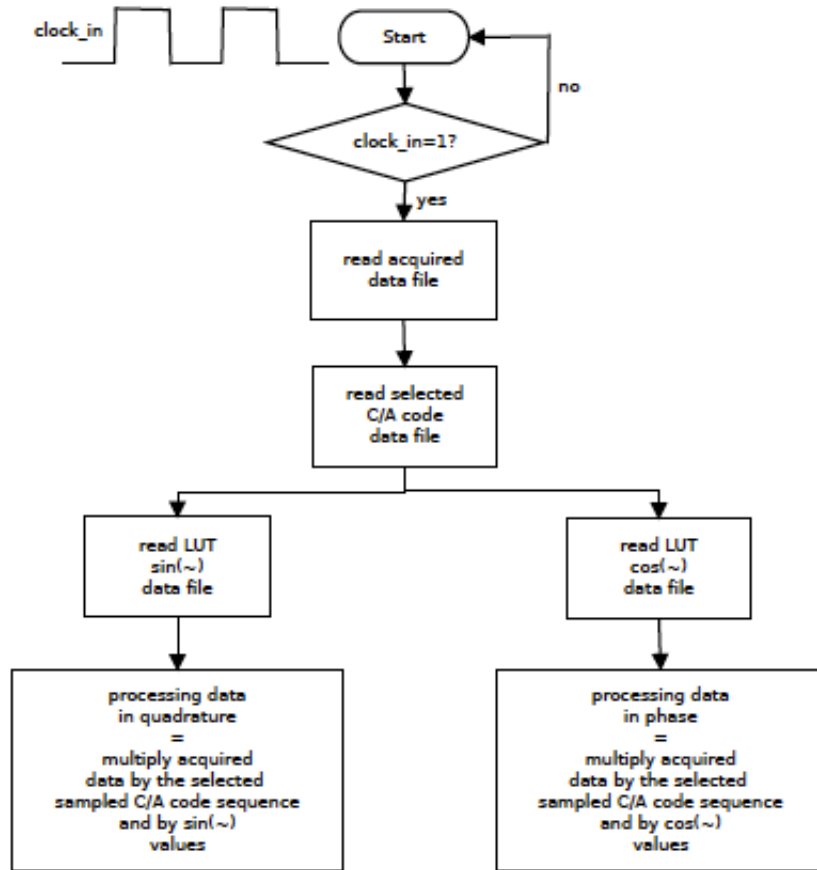
Figure 4.12: Flow diagram: Split in-phase and in-quadrature processing

4.2.1 Split in-phase and in-quadrature processing

As first step, the acquired data has to be multiplied for the 32 sampled C/A codes, obtaining a matrix of 32 rows, one for each C/A code delay. Consequently, the resulting 32 sequences has been multiplied for the $\sin(\cdot)$ LUT and for the $\cos(\cdot)$ (Figure 4.2), in order to obtain the component in-phase and in quadrature (Figure 4.12). Different This procedure has been run considering a range of Doppler frequencies.
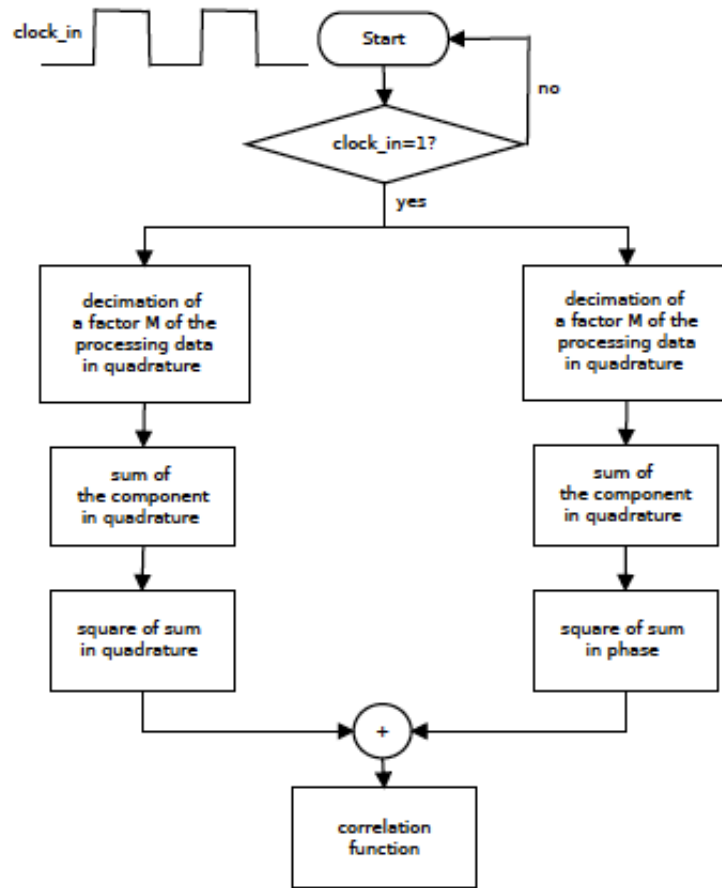
Figure 4.13: Flow diagram: Integrate and Dump

4.2.2 Integrate and Dump

In the Integration and Dump unit, the data are summed to each others recursively dumping every M samples (Figure 4.13). In this work, the design has been tested using three different decimation factor M=16,8,4.

4.2.3 Envelope Detector

To detect the GPS signal has been used the same Envelope Detector used for the FFT Acquisition Unit (Figure 4.9).
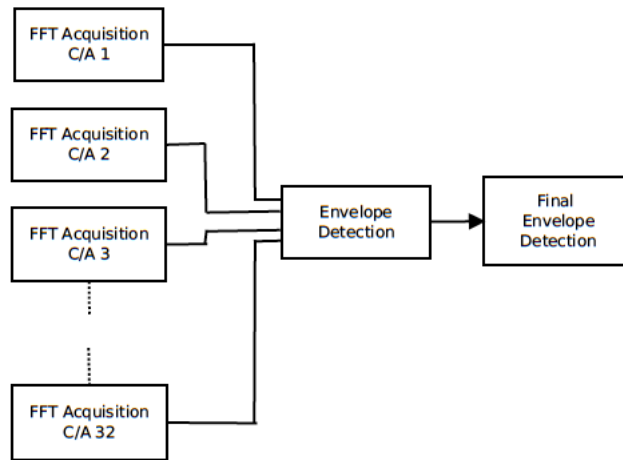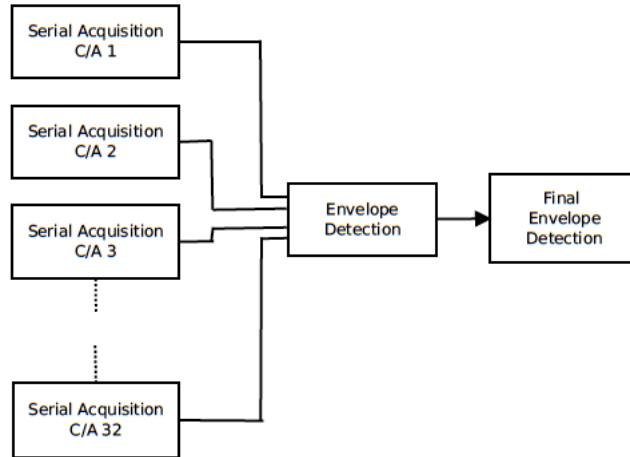
Figure 4.14: Complete design of the Serial Acquisition of the GPS signal for the 32 C/A sequence: block diagram

4.2.4 Final Envelope Detector

The Final Detector is introduced to detect the best Delay-Doppler Map, using the same design presented in the FFT Acquisition Unit (Figure 4.10).

Chapter 5

Acquisition results and comparison

The GNSS reflectometry method has been widely demonstrated to be useful for remote sensing, significant results have been obtained by (Zavorotny et al. [58]), (Gleason et al. [18]). In the measurement of the ocean surface, this method can be considered one of the most interesting, due to the long-term lifetime and to the global coverage (Clarizia et al. [7]). The deleterious effects introduced in the transmission of the GNSS signal causes a reflection on the signal on the scattering surface far from the specular point. This produces a spreading of the received signal power all over the surface in time and frequency. For this reason, a 2-D map of the GNSS signal power on frequency and on time will give a measurement of the transmitted signal. This is important because the detection of a strong signal will produce a better ability of the receiver to remove the noise from the information waveform and make accurate measurement on the reflection surface. In this manuscript, as first step it has been analyzed the received power signal as function of the time to determine if it has been detected the informational signal or just noise. In order to do that, the received data sequence has been detected first with an FFT based acquisition method and then with a serial acquisition technology, both method implemented in VHDL and synthesized on the Xilinx FPGA Virtex 6. These results have been compared with with an acquisition process implemented in Matlab to prove that the hardware designs provide the same results.
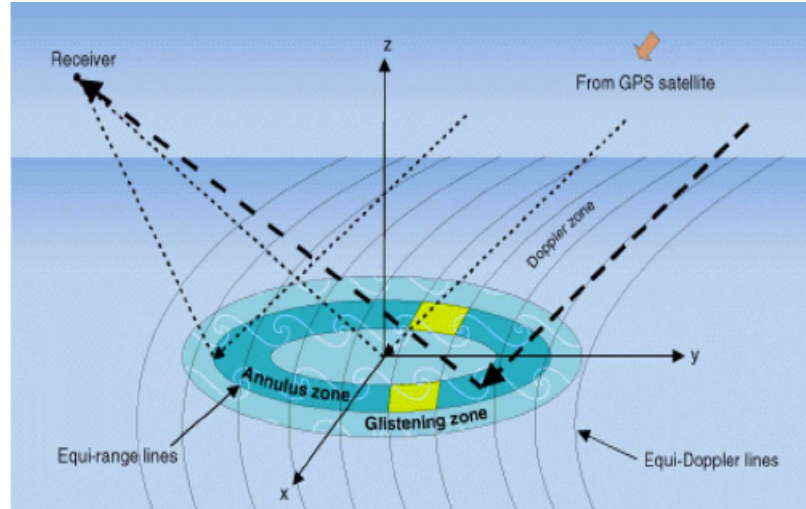
Figure 5.1: GPS reflection geometry over ocean surface (Rodriguez-Alvarez et al. [43])

5.1 The GNSS signal power

The GNSS power signal represents the ability to discriminate the transmitted signal from the noise. More in deep, it is necessary to detect a strong power spike to increase the probability of accurate measurements of the scattering zone. The Specular Point and the zone around it called the Glistening Zone represent a key point for the magnitude of the GNSS reflected power signal (Clarizia et al. [7]). The Glisting Zone is directly proportional to the roughness of the scattering surface. For example, a Glisting Zone on the ocean surface depends increases with the wind speed. Considering a fixed Doppler frequency, the 1-D correlation power waveform of the reflected GNSS signal represents a tool to measure the roughness of the scattering area (Rodriguez-Alvarez et al. [43]). Acquiring 1 ms of data and processing them with the hardware FFT based Acquisition Unit, the GNSS power signal appears as a huge spike around the $5\tilde{0}0$ chips. The same spike has been obtained in both the acquisition unit designed in VHDL and in the acquisition unit implemented in Matlab.
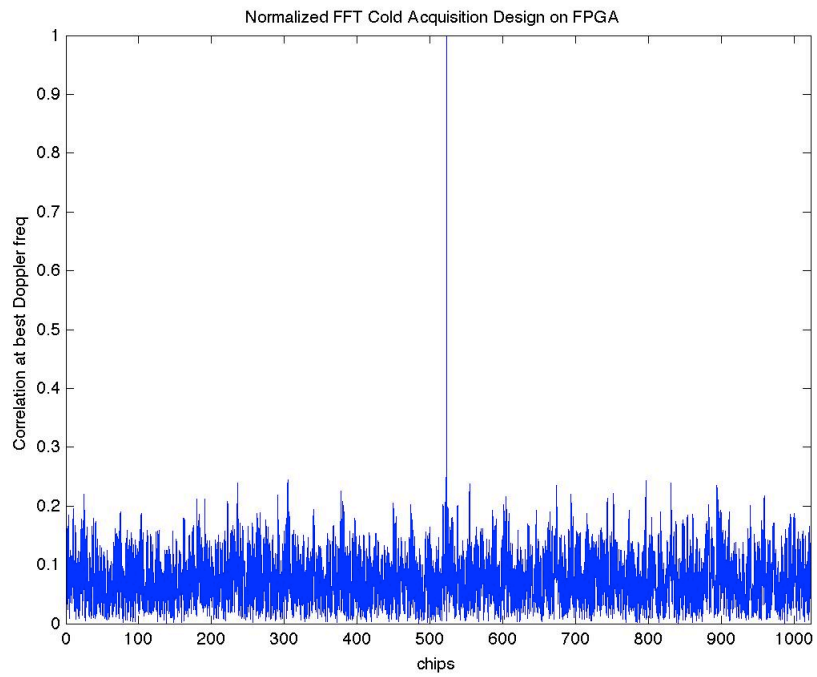
Figure 5.2: Normalized GPS correlation signal with an FFT cold search GPS acquisition in VHDL on FPGA
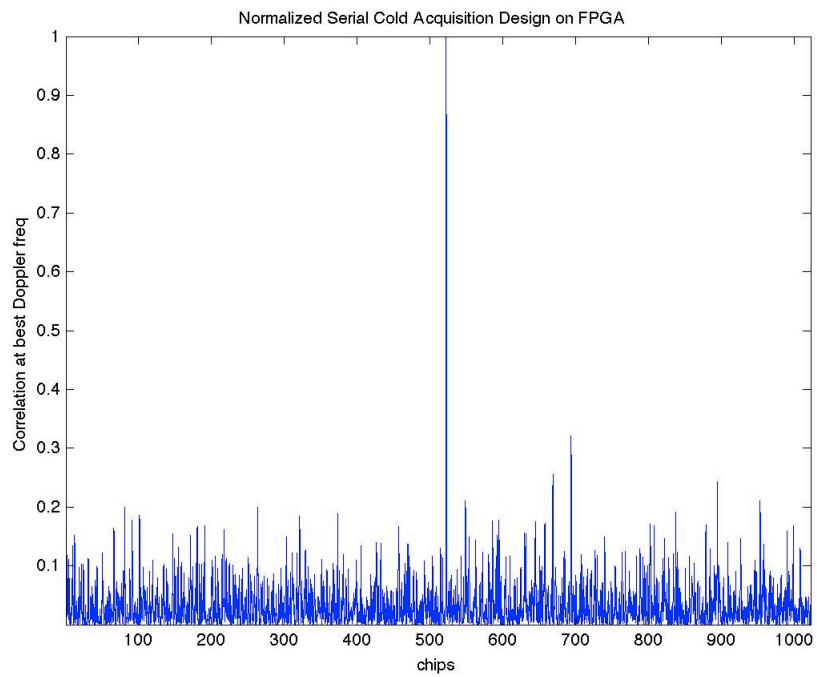
Figure 5.3: Normalized GPS correlation signal with Serial cold search GPS acquisition in VHDL on FPGA
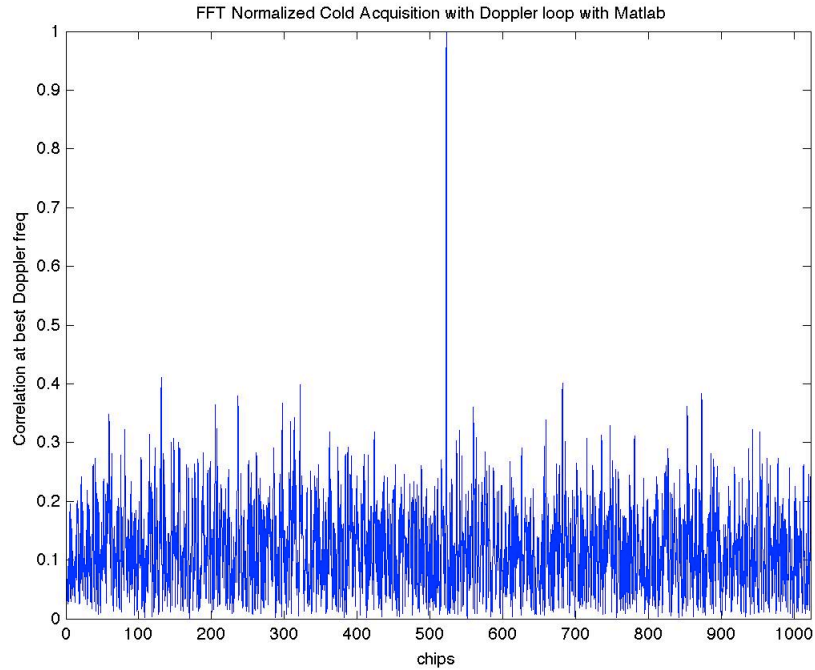
Figure 5.4: Normalized GPS correlation signal with an FFT cold search GPS acquisition in VHDL on Matlab

5.2 Delay Doppler Map: Theoretical Model

The Delay-Doppler Map represents an important tool to study the scattering surface of a GNSS signal. (Zavorotny et al. [58]) developed a model to study the reflection of the GNSS signal on the sea scattering area. In the 2013, (Rodriguez-Alvarez et al. [43]) presented an experiment to study the GNSS-R wind retrievals from an airborne, using a DDM. As first step, the cross-correlation of the components in-phase and in-quadrature of the received signal are respectively multiplied by the PRN sequence of the transmitting satellite for different delays and carrier frequency offsets. Integrating the multiplication of the received waveform and the code replica for a coherent integration time, the cross-correlation is obtained. Averaging a sufficiently number of absolute value of the squared cross-correlation, the DDM can be computed (Rodriguez-Alvarez et al. [43]).

The average of the scattered power results function of delay and Doppler frequency (Clar-

izia et al. [7]), (Zavorotny et al. [58])

$$< Z_x(\tau, f_{dopp}) >\propto \int \int \frac{G_{Rx}(v)}{I_{Tx}^2(v)I_{Rx}^2(v)} \frac{p^4 v}{p_z(v)} S\left(\frac{-p_\perp(v)}{p_z(v)}\right) \chi^2(\tau - \tau_l(v), f_{dopp} - f_l(v))dv$$

(5.1)

where

- G_{Rx} is the receiver antenna gain

- $I_{Tx}(\cdot)$ and $I_{Rx}(\cdot)$ are the path between the reflection point and the transmitter and the receiver, respectively

- v is the vector of the spatial coordinate on the reflection area

- $p(v) = [p_x(v), p_y(v), p_z(v)]$ is the scattering vector

- $S(\frac{-v_\perp(v)}{p_z(v)})$ is the sea surface slope characterized with a two-dimensional zero-mean Gaussian distribution

- $\chi^2(\tau - \tau_l(v), f_{dopp} - f_l(v))$ is the Woodward Ambiguity Function (WAF) of a PR GPS sequence, represented as function of the delay $\tau(v) = [\tau_x(v), \tau_y(v), \tau_z(v)]$ and the Doppler frequency $f_{dopp}(v) = [f_x(v), f_y(v), f_z(v)]$

more in deep, the averaged correlation of the scattered GPS signal power at a given time delay ($\triangle\tau$) and at a given frequency ($\triangle f_{dopp}$) can be represented as (Rodriguez-Alvarez et al. [43])

$$< | Z_x(\triangle\tau, \triangle f_{dopp}) |^2 > = \frac{T_c^2 P_{Tx} G_{Tx} Att \lambda^2}{(4\phi)^3} \times$$
$$\left[\int \int \frac{G_{Rx}(v)\Upsilon^2(\triangle\tau - \tau(v))|Sinc_s(\triangle f_{dopp} - f_{dopp}(v))|^2}{I_{Tx}^2(v)I_{RX}^2(v)} \right] \times$$
$$\phi \mid F \mid^2 \frac{p^4 v}{p_z(v)} P_s\left(\frac{-p_\perp(v)}{p_z(v)}\right) d^2 v$$

(5.2)

where

68

- $\frac{2}{c}$ is the coherent integration time

- $P_{Tx}G_{Tx}$ is the isotropic radiated power effective transmitted

- *Att* is the attenuation introduced from the atmosphere

- $\Upsilon(\tau) = \begin{cases} \frac{1-|\tau|}{L_{chip}} & if \ |\ \tau\ | \leq L_{chip} \\ 0 & otherwise \end{cases}$

- $L_{chip} = \frac{1msec}{1023}$ is the length of the C/A code.

- $Sinc_s = \frac{\sin(\phi f)}{\phi f}\tau(v)$

- F is the Fresnel coefficient

- $P_s(\cdot)$ is the probability distribution function of the ocean surface

In an environment where the wind is present, it is possible to use the spectrum proposed by (Elfouhaily et al. [10]) in addition to the (Zavorotny et al. [58]) model. In the calculation of the DDM is important to know the precise coordinate of the receiver and the transmitter. The DDM is an important tool to study of the reflection surface, but if it is present a significant amount of thermal and speckle noise, it could not be so accurate. In this case, it is important to try to reduce as much as possible the distortions subtracting the noise power from the received signal power (Rodriguez-Alvarez et al. [43]).

Figure 5.5: Delay Doppler Map of the FFT cold search GPS acquisition in VHDL on FPGA (Doppler range $[-200, 200]$ Hz)

Figure 5.6: GPS correlation signal with an FFT cold search GPS acquisition in VHDL on FPGA (Doppler range $[-200, 200]$ Hz)

5.3 Delay Doppler Map

As the GNSS signal reflects on the scattering area, the roughness of that surface causes a spreading of the power signal in time and in frequency. The delay can be calculated dividing the path between the transmitter and the receiver in point. Each point is distant from the next of 1 chip, with a width of 300 m and a duration of $1\mu sec$ (Misra et al. [38]). At the same time, the receiver detects the GNSS signal with a specific Doppler frequency. The GNSS reflected power signal is function of three main factors:

- the roughness of the scattering surface

- the time delay [chips]

- the Doppler frequency [Hz]

For this reason, a 3-D map of the GNSS received signal has been produced. Three different scenarios have been analyzed:

- the ground scenario

- the aircraft scenario

- the spacecraft scenario

In this work, the Delay Doppler Map of the complete acquisition space is plotted, as the velocities get higher this space gets bigger. Instead of the Delay Doppler Map used for remote sensing is always just the smaller area around the GNSS power signal peak. For this reason, even in the space application, it is necessary to scan over a large Delay Doppler space to acquire the signal, but then the remote sensing DDM is still just a small area around the peak.

Figure 5.7: Delay Doppler Map of the FFT cold search GPS acquisition in VHDL on FPGA (Doppler range $[-5000, 5000]$ Hz) in the ground scenario

5.3.1 The Ground Scenario

The **ground scenario** corresponds to the Delay Doppler Map of the reflection process of the GNSS signal studying a reflection path seen by the ground station settled on the Earth. In this case, the Doppler frequency range can be identify in $[-5, +5]$ *kHz*. Processing the received data for this array of values sampled every 500 Hz, the produced DDM shows a GNSS signal centered to the frequency 0 kHz and located around the 500 chips. If the delay array is fixed to the value correspondent to the power signal peak, it is possible to observe that the GNSS signal is the magnitude of a *sinc* function respect to the Doppler frequency range.

72
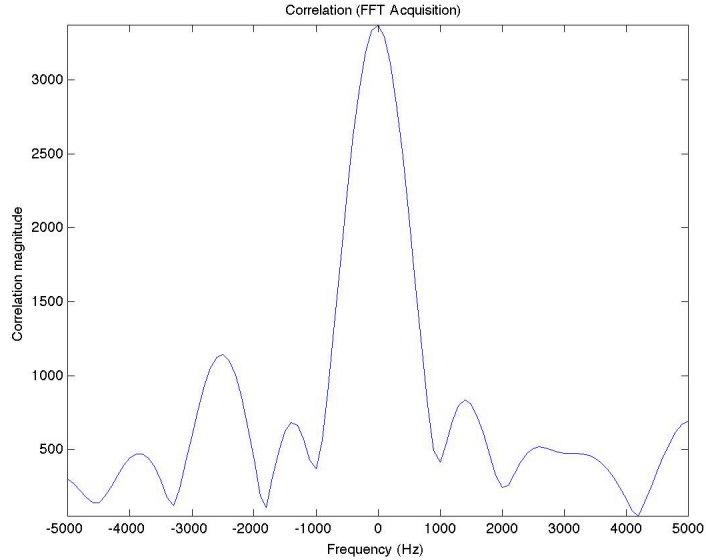
Figure 5.8: GPS correlation signal with an FFT cold search GPS acquisition in VHDL on FPGA (Doppler range $[-5000, 5000]$ Hz) in the ground scenario

5.3.2   The Aircraft Scenario

The second analyzed scenario is the observation of the acquired power signal as function of the time delays and of the Doppler frequencies considering the path from a spacecraft to the receiver through the reflection surface. In this case the Doppler ranges varies in this array of values $[-15, +15]$ *kHz* sampled every 500 Hz. As it is possible to see from the Figure 5.3.2, the produced waveform is still present at the same delay chip and at the same Doppler frequency.
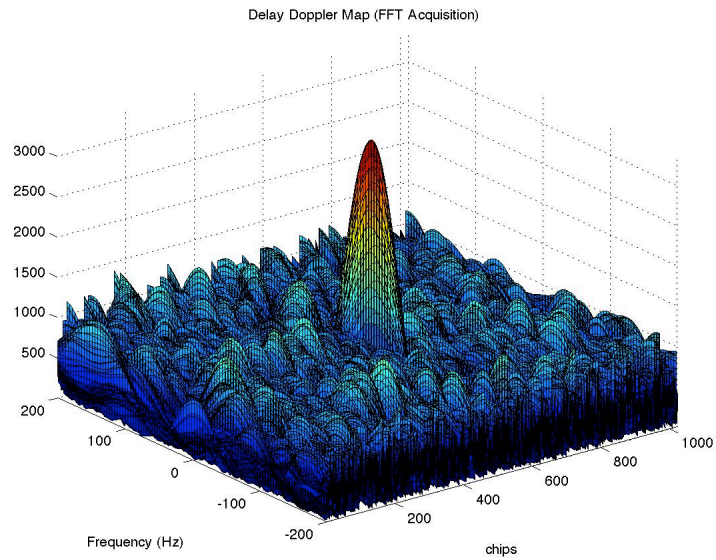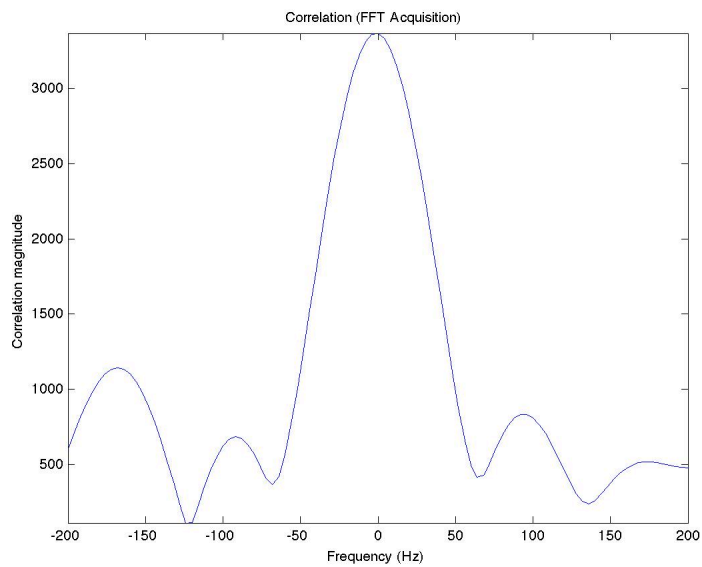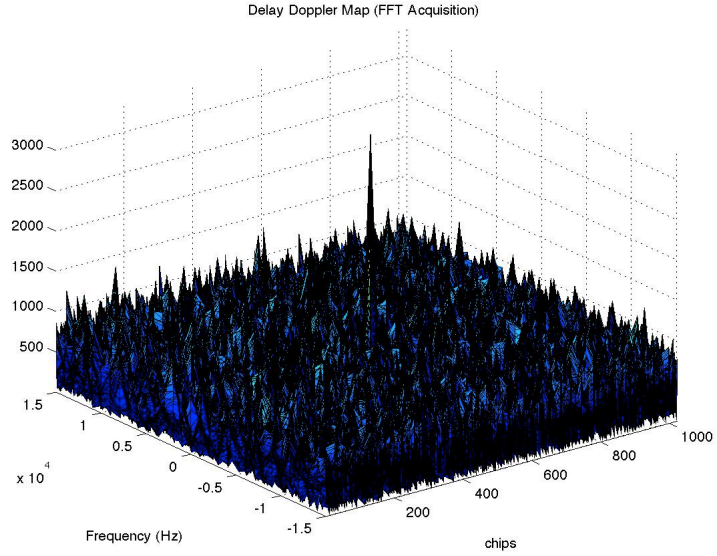
Figure 5.9: Delay Doppler Map of the FFT cold search GPS acquisition in VHDL on FPGA (Doppler range $[-15000, 15000]$ Hz) in the aircraft scenario
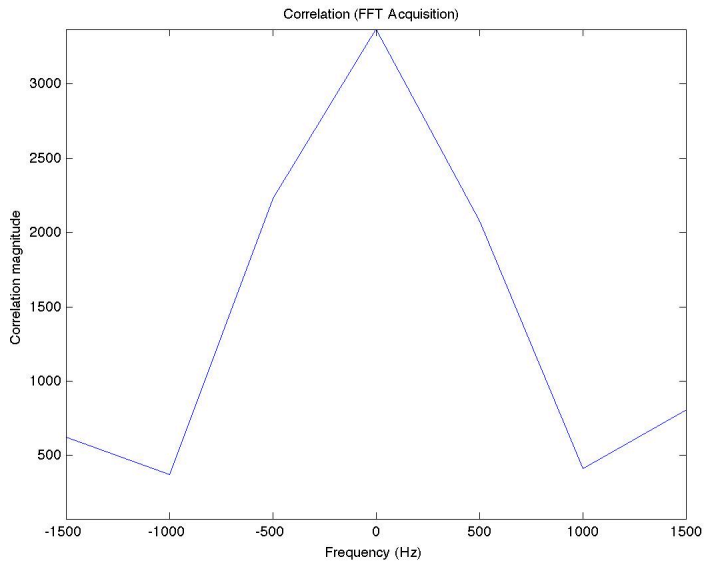
Figure 5.10: GPS correlation signal with an FFT cold search GPS acquisition in VHDL on FPGA (Doppler range $[-15000, 15000]$ Hz) in the aircraft scenario

Delay Doppler Map (FFT Acquisition)

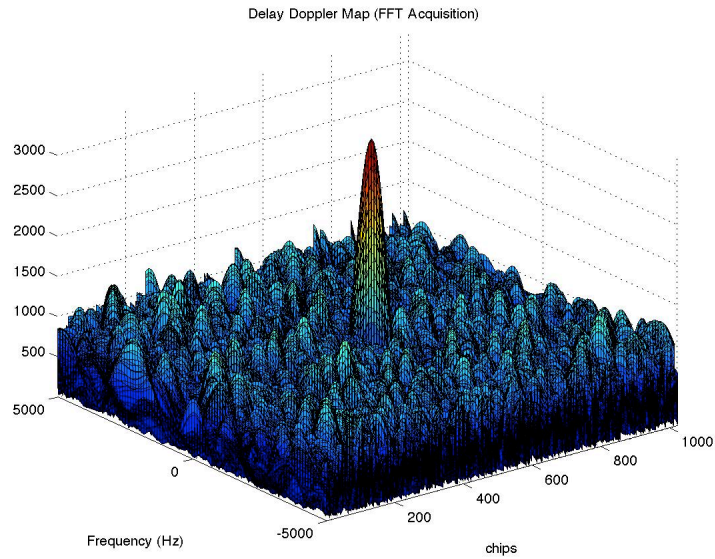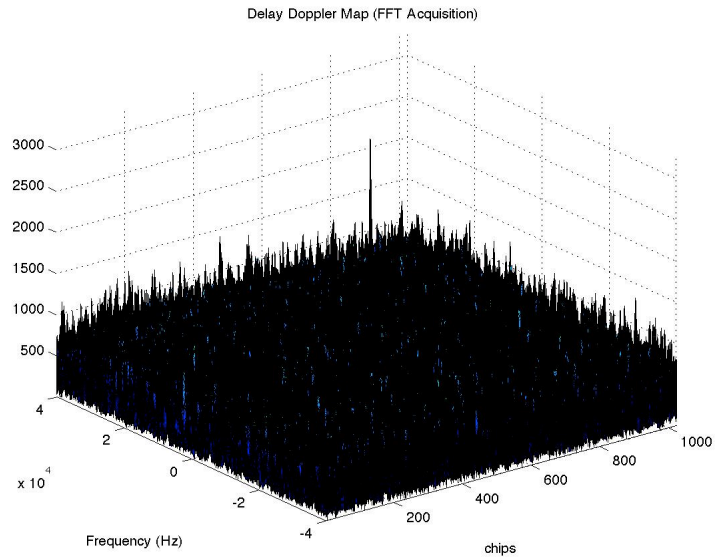Figure 5.11: Delay Doppler Map of the FFT cold search GPS acquisition in VHDL on FPGA (Doppler range $[-40000, 40000]$ Hz) in the spacecraft scenario

5.3.3 The Spacecraft Scenario

The last analyzed scenario considers a space environment with an approximate Doppler frequency range $[-40, +40]$ kHz sampled every 500 Hz. The power signal is still detected even though less visible than in the previous cases.
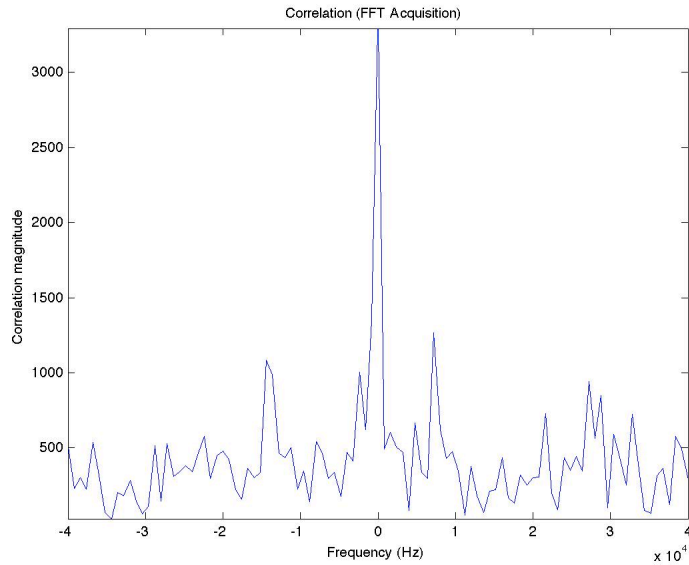
Figure 5.12: GPS correlation signal with an FFT cold search GPS acquisition in VHDL on FPGA (Doppler range $[-40000, 40000]$ Hz) in the spacecraft scenario

All the showed DDMs are obtained, choosing the GNSS power signal with the highest peak of the 32 possible elaborated signals. The highest peak is detected compared all the values of the processed waveforms and storing the waveform with a magnitude at least twice the noise. If the final detector is not introduced and the user choose a random power signal, it is not possible to detect a GPS signal all the time. The final detector is an key-point of the acquisition section, it allows to choose the signal with higher information.

5.4 Obtained Delay-Doppler Map and Delay-Doppler Map of ocean-reflected signals

The design of the DDM for a FPGA device has been done considering 1 ms of acquired data. Detecting the direct signal, the DDM assumes a shapes of concentric circular regions of different colors (Figure 5.13). The GNSS power signal is located in the area with the highest level of red, each zone is represented with a color of the rainbow scale starting form the zone with highest power contribution in red to the one with the lowest power contribution in deep blue. The same DDM can be used to represent GNSS reflected signal on the ocean surface (Figure 5.14).

The ocean-reflected signal collected in the May 21, 2004 (Gleason et al. [21], pp 409, Gleason et al. [18]) has an horseshoe's shape, due to the 1 KHZ of bandwidth and the 1 ms of coherent processing time. The reflected GPS signal depends on the Doppler frequency of the specular point but mainly from two frequencies surrounding the scattering point. As the delay increase, further these two frequencies go. This results in a Delay-Doppler Map with an horseshoe shape.

5.5 Design Performance

The digital design of a circuit is chosen taking care of the used combinational logic in run-time, the timing delay, the maximum operational frequency and the FPGA area allocated. In this project, it has been pay attention in particular on the timing delay. Above it has been listed the performances of the implemented design. As it is possible to notice, the FFT Acquisition Unit presents a lower timing delay even though the chosen pipelined design requires an high allocation areas. Peculiarity of all the pipelined design is the necessity to lose efficiency in the memory area in despite of better time performance. This could represents a problem in case of digital design, as the proposed, with high signal processing
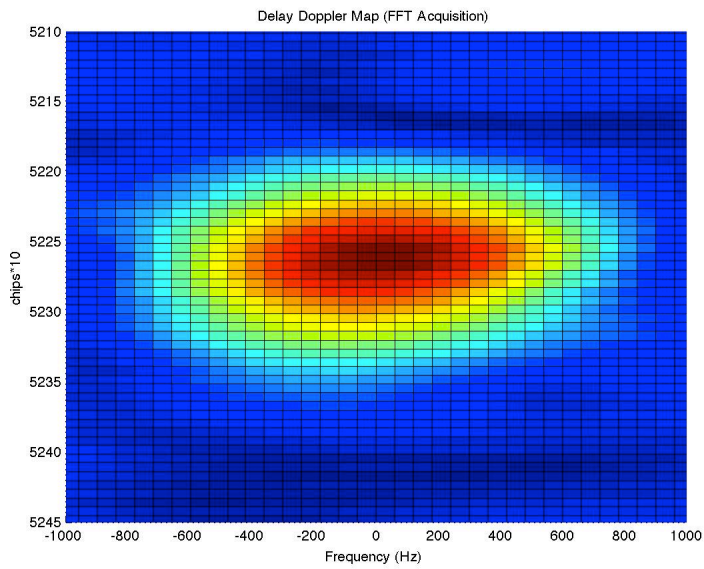
Figure 5.13: Delay Doppler Map obtained with the FFT Acquisition Unit implemented in VHDL
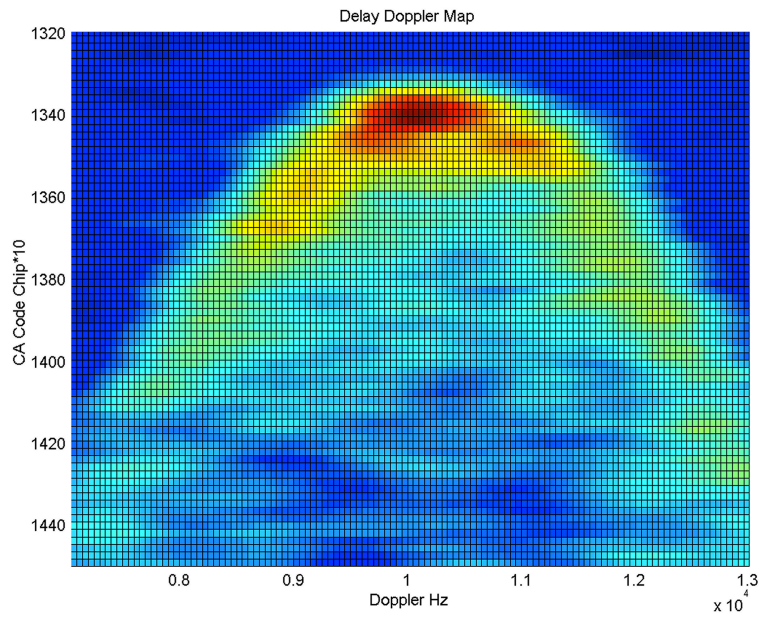
Figure 5.14: Delay Doppler Map of the Ocean reflected signal of GPS satellite PRN 26, found in the May 21, 2004 data set collected by the UK-DMC satellite (Gleason et al. [21], pp 409
)

C/A-Generation-Performances	
Max Delay	$1.443 ns$
f_{max}	$750.188 MHz$

Figure 5.15: C/A code Generation: timing performance

GNSS-FFT-Acquisition-Unit			
	Doppler-range		
	Ground scenario $-5000 : 500 : +5000$ Hz	Aircraft Scenario $-15000 : 500 : +15000$ Hz	Spacecraft Scenario $-40000 : 500 : +40000$ Hz
Max Delay	$80.196 \mu sec$	$232.95 \mu sec$	$614.84 \mu sec$
f_{max}	$427.61 kHz$	$147.21 KHz$	$55.78 KHz$

Figure 5.16: GNSS FFT Acquisition Unit: timing performance

requirements and an available design with lower memory capability.

When an hardware device is used to process date, it is inevitable to incur in limited resources problems. It is the main goal of a good designer to figure out to improve and use at the best the available resource, developing efficient and optimized systems with acceptable performances.

GNSS-Serial-Acquisition-Unit		
Integration and Dump every 4 chips		
Doppler-range		
Ground scenario	*Aircraft Scenario*	*Spacecraft Scenario*
$-5000:500:+5000$ Hz	$-15000:500:+15000$ Hz	$-40000:500:+40000$ Hz
Max Delay	2.352*sec*	6.832*sec*	18.032*sec*
f_{max}	–	–	–

Figure 5.17: GNSS Serial Acquisition Unit with an Integration and Dump Step every 4 chips: timing performance

GNSS-Serial-Acquisition-Unit		
Integration and Dump every 8 chips		
Doppler-range		
Ground scenario	*Aircraft Scenario*	*Spacecraft Scenario*
$-5000:500:+5000$ Hz	$-15000:500:+15000$ Hz	$-40000:500:+40000$ Hz
Max Delay	0.54*sec*	1.708*sec*	4.508*sec*
f_{max}	–	–	–

Figure 5.18: GNSS Serial Acquisition Unit with an Integration and Dump Step every 8 chips: timing performance

GNSS-Serial-Acquisition-Unit Integration and Dump every 16 chips			
	Doppler-range		
	Ground scenario $-5000 : 500 : +5000$ Hz	*Aircraft Scenario* $-15000 : 500 : +15000$ Hz	*Spacecraft Scenario* $-40000 : 500 : +40000$ Hz
Max Delay	$\sim 0.3sec$	$\sim 0.9sec$	$\sim 2.4sec$
f_{max}	$-$	$-$	$-$

Figure 5.19: GNSS Serial Acquisition Unit with an Integration and Dump Step every 16 chips: timing performance

Chapter 6

Future work and Conclusions

The GNSS-Remote Sensing is an innovative technology for ocean and land sensing, for cryosphere mapping. The low-cost and the several advantages of this system have facilitated the diffusion of the GNSS network on all the globe. The increasing number of GNSS satellites will intensify the GNSS network improving the resolution of the atmosphere's monitoring. Advanced GNSS ground stations will be able to capture in line-of-sight the signals transmitted from the multi-frequency GNSS satellite constellations. The American GPS, the Russian GLONASS, the European GALILEO and the Chinese COMPASS are all moving forwards to develop accurate systems able to measure and track hydrology and climate processes as well as oceanographic and atmospheric events using GNSS satellites as transmitter and aircraft or LEO (*Low Earth Orbit*) satellite as receiver (Gleason et al. [21]).

The high accuracy of these new systems requires innovative algorithm with high performance in terms of timing analysis and measures resolutions. Due to the requirements and to the complexity of the GNSSs the possibility to process the data on a re-configurable hardware device, as an FPGA could respect the required specifications of this systems. The advantages of a re-configurable technology reside in providing accurate results in short time with a low-cost, a reduced device's occupied area and low power consumption (Girau

et al. [17]).

The FPGAs are relatively simple to program but in order to achieve the wished performances, it is necessary to pay attention to the system's design. Working with an hardware devices means to make some compromise. In this work, the main goal was to achieve high timing performances and accurate measurements of the scattered signal using the Delay Doppler Map with the design of the FFT based acquisition unit and the serial acquisition unit, respectively. The design of the acquisition unit with different algorithm and different delay chips resolution has shown how it is possible to easily manage an re-programmable hardware system based on the requirements of the users.

Due to the necessity of quasi real-time data processing, high performing GNSS receivers are required. The performances of the obtained design could be improved making the FPGA algorithms run in real-time and and optimization of the number of parallel reflections that can be mapped. Nowadays, the multi-antenna GNSS TriG

(*Tri-GNSS, GPS+Galileo+Glonass*) receiver is being developed by the JPL *Jet Propulsion Laboraty*. Earlier, the JPL developed the Blackjack GPS receiver widely used in several GNSS missions for the radio occultation and orbit measurements (Montenbruck et al. [37]). On the other side, the ICE (*IEEC-CSIC Spain*) is conducting research in high-performing instruments for the multi-frequency GNSS systems. Previously, the griPAU (*GNSS Reflectometer Instrument for the Passive Advanced Unit*) project has been developed in the Universitat Politcnica de Catalunya. This device has been used to perform measurements on soil moisture and ocean taking advantage from the GPS signal's reflection, increasing the accuracy of the measurements(Valencia et al. [50]).

Another interesting project is the SGR-ReSI (*Space GPS Receiver-Remote Sensing Instrument*) for the study of GNSS-Remote Sensing on ocean, land and atmosphere (Unwin et al. [48]). The SGR-ReSI is conducted by the University of Bath, the Surrey Space Centre (University of Surrey) and the National Oceanography Centre.

In the upcoming years, several Shuttle based experiments are scheduled to study the GPS

reflectometry and refractometry using the last GNSS Receiver-Remote Sensing Instrument. In addition, other innovative idea about the GNSS Radio Occultation receiver will be realized.

Bibliography

[1]   Armatys, M., *Estimation of Sea Surface Winds Using Reflected GPS Signals*, Ph.D. thesis, University of Colorado, 2001.

[2]   Belmonte Rivas, M., Maslanik, J. A., Axelrad, P., *Bistatic Scattering of GPS Signals Off Arctic Sea Ice*, IEEE Transactions on Geoscience and Remote Sensing, Vol. 48, No. 3, March 2010

[3]   Botros, N. M., *HDL Programming Fundamentals: VHDL and Verilog*, Da Vinci Engineering Press, 2005

[4]   Cardellach, E., Ruffini, G., Pino, D., Rius, A., Komjathy, A., Garrison, J.L., *Mediterranean Balloon Experiment: ocean wind speed sensing from the stratosphere, using GPS reflections* Remote Sensing of Environment, 88: 351-362, 2003

[5]   Cardellach, E., Rius, A., *A New Technique to Sense Non-Gaussian Features of the Sea Surface From L-band Bi-Static GNSS Reflections*, Remote Sensing of Environment, 112, 2008, pp. 2927-2937

[6]   Chao, Y., *Modeling the Gulf Stream System: How far From Reality?*, Geophys. Res. Lett., 23, 3155-3158, 1996

[7]   Clarizia, M. P., Gommenginger, C. P., Gleason, S. T., Srokosz, M. A., Galdi, C., Di Bisceglie, M., *Analysis of GNSS-R delay-Doppler maps from the Uk-DMD satellite over the ocean*, Geophysical Research Letters, Vol. 36, 2009.

[8]   Clifford, C.F., Tatarskii, V.I., Voronovich, A.G. Zavorotny, V.I., *GPS Sounding of Ocean Surface Waves: Theoretical Assessment*, Proceedings of the IEEE International Geosciences and Remote Sensing Symposium: Sensing and Managing the Environment, IEEE, Piscataway, NJ, 2005-2007, 1998.

[9]   Department of Defence USA, GPS Navistar, *GLOBAL POSITIONING SYSTEM STANDARD POSITIONING SERVICE PERFORMANCE STANDARD*, 4th edition, September 2008

[10]   Elfouhaily, T. M., et al., *A Unified Directional Spectrum for Long and Short Wind-Driven Waves*, Journal of Geophysical Research, Vol. 102, No.. C7, July 15, 1997, pp. 15781-15796

[11]   El-Rabbany, A., *Introduction to GPS : the Global Positioning System*, mobile communication series, 2002.

[12]   Francis, R. J., *A Tutorial on Logic Synthesis for Lookup-Table Based FPGAs*,IEEE, 1992, $O - 8186 - 3010 - 8/92$

[13]   Garrison, J.L., Katzberg, S.J. Howell, C.T., *Detection of Ocean Reflected GPS Signals: Theory and Experiment*, Proc. the IEEE Southeast, Blacksburg, USA, 12-14 April, pp. 290-294, 1997.

[14]   Garrison, J.L. Katzberg, S., *The application of reflected GPS signals to ocean and wet land remote sensing*, In the Proceedings of the Fifth International Conference on Remote Sensing for Marine and Coastal Environments, San Diego, CA, 5-7 October, Vol. 1, pp. 522-529, 1998.

[15]   Garrison, J.L. Katzberg, S., *The Application of Reflected GPS Signals to Ocean Remote Sensing*, Remote Sensing of Environment, Volume 73, Issue 2, August 2000, Pages 175187.

[16]   Garrison, J.L., Komjathy, A., Zavorotny, V.U., Katzberg, S.J., *Wind Speed Measurement Using Forward Scattered GPS Signals*, IEEE Transactions on Geoscience and Remote Sensing, 40(1): 50-65, 2002.

[17]   Girau, G.,Tomatis, A., Dovis, F., Mulassano, P., *Efficient Software Defined Radio Implementations of GNSS Receivers*, IEEE, 2007

[18]   Gleason, S., Hodgart, S., Sum, Y., Gommenginger, C., Macking, S., Adjrad, M.M., Unwin, M., *Detection and Processing of Bistatically Reflected GPS Signals From Low Earth Orbit for the Purpose of Ocean Remote Sensing*, IEEE Transactions on Geoscience and Remote Sensing, Vol. 43, No.6, June 2005

[19]   Gleason, S., *Remote Sensing of Ocean, Ice and Land Surfaces Using Bistatically Scattered GNSS Signals From Low Earth Orbit*, Ph.D. thesis, University of Surrey, United Kindom, 2006.

[20]   Gleason, S., *Reflecting on GPSs: Sensing Land and Ice From Low Earth Orbit*, GPS World, October 2008.

[21]   Gleason, S., Gebre-Egziabher, D., *GNSS Technology and Applications Series*, Arthech House, 2009.

[22]   Gleason, S., *Towards sea ice remote sensing with space detected GPS signals: demonstration of technical feasibility and initial consistancy check with low resolution sea ice information*, Remote Sensing 2, 2017-2039, 2010

[23]   Kaplan, E. D., *UNDERSTANDING GPS : Principles and Applications*, Artech House Publishers, 1996.

[24]   Kappen, G., Noll, T. G., *Application specific instruction processor based implementation of a GNSS receiver on an FPGA*, Design, Automation and Test in Europe, 2006

[25]   Katzberg, S.J. , Torres, O., Grant, M.S., Masters, D., *Utilizing calibrated GPS reflected signals to estimate soil reflectivity and dielectric constant: Results from SMEX02*, Remote Sens. Environm., 100:17-28, 2005

[26]   Komjathy, A., Maslanik, J. A., Zavorotny, V. U., Axelrad, P., Katzberg, S. J., *Sea Ice Remote Sensing Using Surface Reflected GPS Signals*, Proceedings of the IEEE international Geosciences and Remote Sensing Symposium (IGARSS 2000), Honolulu, Hawaii, 24-28 July, 2855-2857, 2000

[27]   Komjathy, A., et al., *Retrieval of Ocean Surface Wind Speed and Wind Direction Using Reflected GPS Signals*, J. Atmos. Ocean. Tech., 21(3), 2004, pp. 515-26

[28]   Hall, C., and R. Cordy, *Multistatic Scaterrometry*, Proceedings of the IEEE International Geoscience and Remote Sensing Symposium, Edinburgh, Scotland, 1988.

[29]   Hofmann-Wellenhof, Lichtenegger, Wasle, *GNSS: Global Navigation Satellite Systems GPS, GLONASS, Galileo and more*, Springer Wien New York, 2008.

[30]   ARINC Engineering Services, LLC, *Navstar global Positioning System, **Interface Specification IS-GPS-200**, Revision D, 7 December 2004, Navstar GPS Space Segment/Navigation User Interfaces*, Space and Missile Systems Center (SMC), Navstar GPS Joint Program Office (SMC/GP).

[31]   Lanzagorta, M., Bique, S., Rosenberg, R., *Introduction to Reconfigurable Supercomputing*, Mark D. Hill, University of Wisconsin, Madison, 2010

[32]   Larson K., Axelrad, P., ASEN 5090 Lecture Slides, University of Colorado

[33]   Lowe, S., et al., *5 ms Precision Aircraft Ocean Altimetry Using GPS Signals*, Geophysical Research Letters, Vol. 29, No. 10, 2002.

[34] Martin-Neira, M., *A Passive Reflectometry and Interferometry System (PARIS): Application to Ocean Altimetry*, ESA Journal, Vol. 17, 1993 U.S. Patent 5 546 087, Aug. 13, 1996.

[35] Martin-Neira, M., Caparrini, M., Font-Rosselo, J., et al., *The PARIS concept: An experimental demonstration of sea surface altimetry using GPS reflected signals*, IEEE Transactions on Geoscience and Remote Sensing, 39: 142-150, 2001

[36] Master, D., *Surface Remote Sensing Applications of GNSS Bistatic Radar: Soil Moisture and Aircraft Altimetry*, Ph.D. thesis, University of colorado, 2004

[37] Montenbruck, O., Kroes, R., *In-flight Performance Analysis of the CHAMP BlackJack Receiver*, GPS Solutions 7, 74-86, 2003

[38] Misra, P., Enge, P., *GLOBAL POSITIONING SYSTEM Signals, Measurements, and Performance*, Ganga-Jamuna Press, 2nd edition.

[39] Proakis, J.G., Salehi, M., *COMMUNICATION SYSTEMS ENGINEERING*, Pearson Education International, 2nd Ed.

[40] Ruf, C. AOSS Dept., Univ. of Michigan, Ann Arbor, MI, USA, Gleason, S. ; Jelenak, Z. ; Katzberg, S. ; Ridley, A. ; Rose, R. ; Scherrer, J. ; Zavorotny, V., *The NASA EV-2 Cyclone Global Navigation Satellite System (CYGNSS) mission*, Aerospace Conference, 2013 IEEE

[41] Janathan Rose, Alberto Sangiovanni-Vincentelli, *Architecture of Field-Programmable Gate Arrays*, IEEE, 1993

[42] Ruffini, G., et al., *The Eddy Experiment: Accurate GNSS-R Ocean Altimetry from Low Altitude Aircraft*, Geophysical Research Letters, Vol. 31, No. 21, June 2004.

[43] Rodriguez-Alvarez, N., Akos, D. M., Zavorotny, V. U., Smith, J. A., Camps, A., Fairwall, C. W., *Airborne GNSS-R Wind Retrievals Using Delay-Doppler Maps*, IEEE Transactions on Geoscience and Remote Sensing, Vol. 31, No. 1, January 2013.

[44] Schmidt, T., Wickert, J., Haser, A., *Variability of the upper troposphere and lower stratosphere observed with GPS radio occultation bending angles and temperatures*, Advances in Space Research, 46, 2, 150-161, 2010

[45] Smith, R. D., et al., *Numerical Simulation of the North Atlantic Ocean at* $1/10^o$, J. Phys. Oceanogr., 30, 1532-1561, 2000

[46] Soulat, F., *Sea Surface Remote Sensing With GNSS and Sunlight Reflections*, PhD thesis, Universitat Politecnica de Catalunya, Spain, 2004

[47] Thompson, D. R., Elfouhaily, T. M., Garrison, J. L., *An improved geometrical optics model for bistatic GPS scattering from the ocean surface*, IEEE Transactions on Geoscience and Remote Sensing, 43(12), 2810-2821, 2005

[48] Unwin, M., de Vos van Steenwijk, R., Gommenginger, C., Mitchell, C., Gao, S., *The SGR-ReSI- A New Generation of Space GNSS Receiver for Remote Sensing*, 23rd International Technical Meeting of the Satellite Division of the Institute of Navigation 2010, ION GNSS 2010. Fairfax, VA.: Institute of Navigation, pp. 1061-1067

[49] Van Nee, D. J. R., and A. J. R. M. Coenen, *New Fast GPS Code-Acquisition Tecnique using FFT*, Electronics Letters, Vol. 27, January 1991

[50] Valencia, E., Camps, A., Marchan-Hermandez, J.F., Bosch-Lluis, X., Rodriguez-Alvarez, N., Ramos-Perez, I., *Advanced architectures for real-time Delay-Doppler Map GNSS-reflectometers: the GPS reflectometer instrument for PAU (griPAU)*, Advanced Space Research 46(2) 196-207

[51]   Van Diggelen, F., *A-GPS: Assisted GPS, Gnss, and Sbas*, Arthech House, 2009

[52]   Xilinx, *Virtex-4 Family Overview*, DS112 (v3.1) August 30, 2010

[53]   Xilinx, *Virtex-5 Family Overview*, DS100 (v5.0) February 6, 2009

[54]   Xilinx, *Virtex-6 Family Overview*, DS150 (v2.4) January 19, 2012

[55]   Xilinx, *LogiCORE IP Fast Fourier Transform v7.1, Product Specification*, DS260
        March 1, 2011

[56]   Xilinx, *XC4000E and XC4000X Series Field Programmable Gate Arrays*, May 14,
        1999 (Version 1.6)

[57]   Yunck, T.P., *The Promise of Spaceborne GPS for Earth Remote Sensing*, Presentation
        at the International Workshop on GPS Meteorology, Tsukuba, Japan, 14-16 January
        2003.

[58]   Zavorotny, V. U., and A. G. Voronovich, *Scattering of GPS Signals from the Ocean
        with Wind Remote Application*, IEEE Transactions on Geoscience and Remote
        Sensing, Vol. 38, No. 1, March 2000, pp. 951-964

[59]   *www.gps.gov/systems/gps/space/*

[60]   *www.gps.gov/systems/gps/control/*

[61]   *www.russianspaceweb.com/uragan.html*

[62]   *www.esa.int*

[63]   *http://home.mit.bme.hu/ szedo/FPGA/fpgahw.htm*

[64]   *http://www.embeddedtechmag.com/component/content/article/7544?start=1*